



# Divergence-time estimates for hominins provide insight into encephalization and body mass trends in human evolution

Hans P. Püschel<sup>1</sup>✉, Ornella C. Bertrand<sup>1</sup>, Joseph E. O'Reilly<sup>2</sup>, René Bobe<sup>1,3,4</sup> and Thomas A. Püschel<sup>1,3</sup>✉

**Quantifying speciation times during human evolution is fundamental as it provides a timescale to test for the correlation between key evolutionary transitions and extrinsic factors such as climatic or environmental change. Here, we applied a total evidence dating approach to a hominin phylogeny to estimate divergence times under different topological hypotheses. The time-scaled phylogenies were subsequently used to perform ancestral state reconstructions of body mass and phylogenetic encephalization quotient (PEQ). Our divergence-time estimates are consistent with other recent studies that analysed extant species. We show that the origin of the genus *Homo* probably occurred between 4.30 and 2.56 million years ago. The ancestral state reconstructions show a general trend towards a smaller body mass before the emergence of *Homo*, followed by a trend towards a greater body mass. PEQ estimations display a general trend of gradual but accelerating encephalization evolution. The obtained results provide a rigorous temporal framework for human evolution.**

Establishing a timescale for human evolution is of essential relevance in palaeoanthropology<sup>1–3</sup> because reliable estimates of the timing of speciation events across the hominin phylogeny facilitate the correlation of these events with both abiotic and biotic processes on geological timescales. An accurate timescale also provides a framework to test for associations between landmark evolutionary changes and different putative extrinsic causal factors such as changes in climate or other environmental influences<sup>4,5</sup>. Despite recent relevant fossil findings, the antiquity and emergence of the genus *Homo*, as well as the timing of the divergence of our lineage with other African apes, have not found a consensus<sup>6–9</sup>.

Traditionally, palaeoanthropologists have used maximum parsimony analysis to infer hominin phylogenetic relationships<sup>10–12</sup> but this approach does not explicitly estimate divergence times as part of the estimation of the phylogeny. Previous studies<sup>13,14</sup> computed confidence intervals for the disappearances and appearances of several hominins. However, their approach is not easily applicable to several available hominin taxa, as it requires the availability of extensive palaeontological datasets. Additionally, this method only provides confidence intervals for local first- and last-appearance data, which do not correspond to the global origination and extinction dates of the taxa under analysis. Other studies have computed these values but their results have been limited by either focusing on a restricted number of hominin taxa<sup>2</sup> or because the assumptions of their applied methods were not met<sup>15</sup>. Bayesian phylogenetic inference methods have also been applied to morphological data<sup>16,17</sup> to provide divergence-time estimates. However, these estimates were exclusively based on anatomical data, even though it is now widely known that the fragmentary nature of the fossil record is not enough to compute reliable divergence estimates<sup>18</sup> and that it is necessary to

consider the molecular information available for several hominin and ape taxa in the analyses.

There is currently a consensus that the most feasible way of determining an accurate evolutionary timescale is by using the molecular clock, a prospect that has progressively concretized with the development of Bayesian relaxed clock methods<sup>19–22</sup>. Bayesian divergence-time estimates require the use of prior probability distributions to incorporate fossil evidence for calibrating the tree. Recently, a new approach known as total evidence dating (TED), tip-dating or integrative dating<sup>23</sup> has been developed<sup>24,25</sup>. TED complements the molecular sequence data derived from extant species with morphological information from both living and extinct species, which allows a more thorough inclusion of fossil data in the analysis and estimation of divergence times.

Hence, in this work we applied this divergence-time estimation method to produce total evidence evolutionary timescales for the hominin clade. We considered four different topological hypotheses with alternative reasonable affinities for problematic hominin taxa (Fig. 1). This is highly relevant because these timescales can be used for dating the origin of *Homo* or any other hominin genus, inferring evolutionary rates and patterns, as well as providing a better understanding of the co-evolution of hominins and their environment. Additionally, we subsequently used the dated trees to carry out ancestral state reconstructions (ACSR) of two evolutionary important phenotypic characters: body mass and phylogenetic encephalization quotient (PEQ). Body mass affects almost every aspect of an animal's biology and ecology<sup>26,27</sup>, hence its importance in any palaeobiological inference, whilst an evolutionary trend of increasing encephalization is one of the hallmark processes in human evolution<sup>28,29</sup>.

<sup>1</sup>School of GeoSciences, University of Edinburgh, Grant Institute, Edinburgh, UK. <sup>2</sup>MRC Human Genetics Unit, MRC Institute of Genetics & Molecular Medicine, University of Edinburgh, Western General Hospital, Edinburgh, UK. <sup>3</sup>Primate Models for Behavioural Evolution Lab, Institute of Cognitive and Evolutionary Anthropology, School of Anthropology and Museum Ethnography, University of Oxford, Oxford, UK. <sup>4</sup>Gorongosa National Park, Sofala, Mozambique. ✉e-mail: [H.P.Puschel-Rouliez@sms.ed.ac.uk](mailto:H.P.Puschel-Rouliez@sms.ed.ac.uk); [thomas.puschelroulez@anthro.ox.ac.uk](mailto:thomas.puschelroulez@anthro.ox.ac.uk)

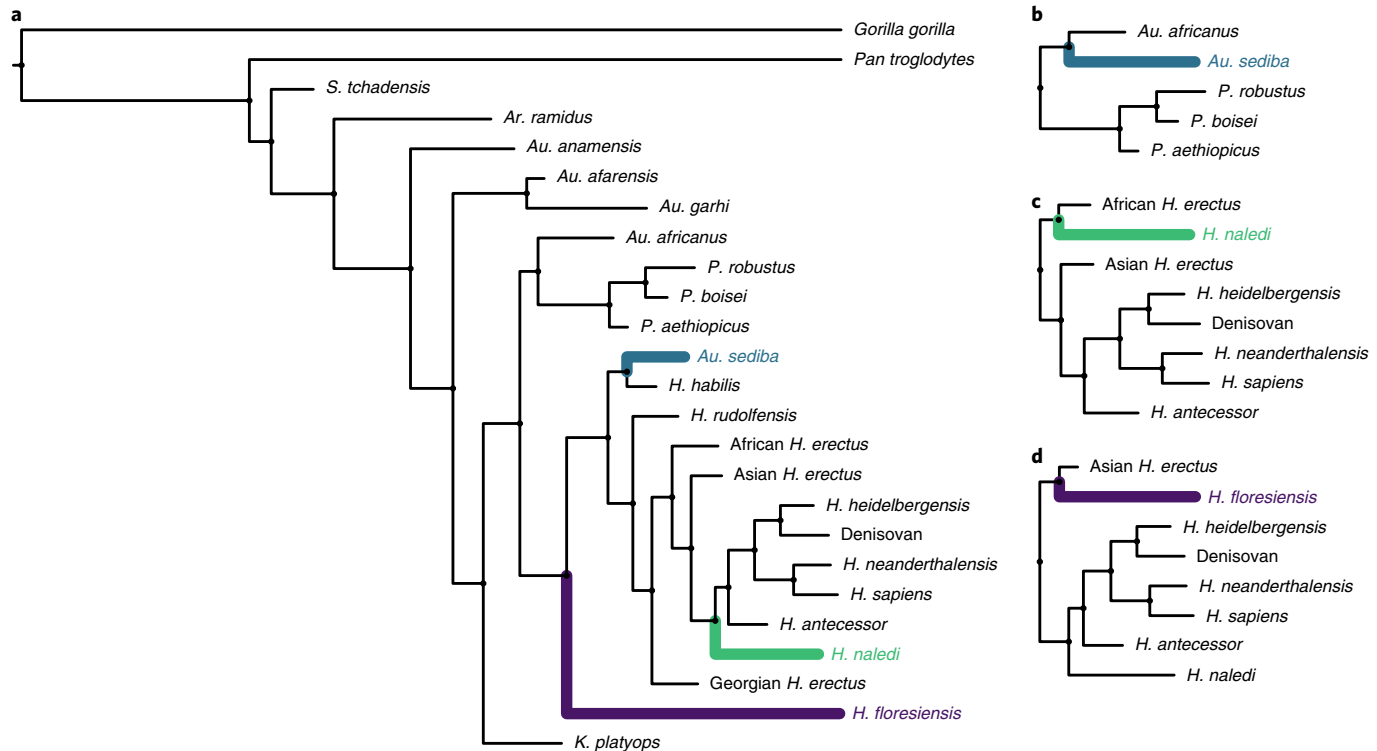


**Fig. 1 | Alternative topological hypotheses tested in the TED analyses.** **a**, Similar to the phylogeny of Dembo et al.<sup>17</sup>. **b**, The same topology as **a** but moving *Au. sediba* from the *Homo* clade to be the sister taxon to *Au. africanus*. **c**, The same topology as **a** but changing the position of *H. naledi* from the stem of *H. antecessor* and its closest *Homo* relatives to be the sister taxon to the African *H. erectus*. **d**, The same topology as **a** but taking *H. floresiensis* from its basal position within the genus *Homo* to be the sister taxon to the Asian *H. erectus*.

## Results

The TED analyses (Fig. 2, Extended Data Fig. 1 and Table 1) show, in general, better-resolved divergence times for the nodes that have both morphological and molecular information available, in comparison with the nodes estimated with morphological information alone. The common ancestor of hominins and *Pan troglodytes* (node 2) was dated at ~7.5 million years ago (Ma) with an uncertainty range of 8.59–6.61 Ma considering the 95% highest posterior density intervals (HPD) of all the trees. The common ancestor of the genus *Homo* (node 13 or 14 for *H. floresiensis* hypothesis) was dated at ~3.3 Ma with an uncertainty range of 4.30–2.56 Ma considering the 95% HPD of all the trees. In general, estimations for this node were consistent between the four trees, although the biggest difference resulted when *H. floresiensis* is removed from the base of *Homo*, making the node's age slightly younger (Fig. 2d). The prior sensitivity analysis (Extended Data Fig. 2) shows mostly minor differences between divergence times in the original analysis and analyses using different priors in relevant parameters, suggesting that the TED analyses are robust to changes in the priors used.

The maximum likelihood (ML) ACSR based on the four consensus trees (Figs. 3 and 4 and Extended Data Figs. 3–6) are consistent with the ACSR based on samples of the posterior trees from these analyses (Fig. 5 and Extended Data Fig. 7). The main difference is an apparent PEQ overestimation in the case of the ACSR based on the consensus trees versus the ACSR based on samples of the posterior trees (Fig. 5). This is because using equations based on PGLS regressions of the consensus trees (Extended Data Fig. 8) returned lower expected brain masses calculated for the trees' tips on average than equations based on the sampled trees (Extended Data Fig. 9). However, the general PEQ trends remain the same. Similarly, the brain mass ACSR versus body mass ACSR results show

a consistently similar pattern for the four analyses. When we analyse all the nodes together in the four trees, the slopes are slightly positive and the  $R^2$  values are low (~0.11) (Extended Data Fig. 10a–d). However, when we split the data there are clearly two different trends. Before node 13/14 the slopes are negative with a moderate  $R^2$  (~0.46) (Extended Data Fig. 10e–h), whereas after node 13/14 the slopes are strongly positive with a high  $R^2$  (~0.96) (Extended Data Fig. 10i–l).

The speciation events since the divergence from *Gorilla gorilla* to the common ancestor of *Homo* (nodes 1–9 and 13/14), all occurred within the latest Miocene and Pliocene (Fig. 2 and Table 1). For that period, the body mass ACSR show that from a common ancestor of ~71 kg at 10.4 Ma, there is a trend of rapid decrease in body mass reaching around 38 kg by 3.3 Ma (Figs. 3 and 5a–d and Extended Data Fig. 5). That is 1.87 times smaller in 7.1 Myr. However, the PEQ ACSR show an opposite trend, increasing from ~0.87 to 1.88 in the same period (Figs. 4 and 5e–h and Extended Data Fig. 6), which is 2.16 times greater. The effect of removing of *H. floresiensis* from the base of *Homo* (Figs. 4d and 5h and Extended Data Fig. 6d) is a higher estimated PEQ for the last common ancestor of this genus (2.16) and the surrounding nodes. Following the path leading to *Australopithecus africanus* and the members of the genus *Paranthropus* (nodes 1–10) the body mass tends to decrease to ~37 kg at node 10, which means a reduction of 1.92 times from the root in 6.6 Myr. Nevertheless, the path from nodes 9 to 10 does not indicate an increase in PEQ. Instead, it corresponds to the beginning of a slight reduction in PEQ in the lineage leading to *Paranthropus*. Interestingly, the last member of this genus, *P. robustus*, displays an increase in PEQ just before the extinction of the lineage. The incorporation of *Au. sediba* as the sister taxon of *Au. africanus* did not have a substantial influence on the ACSR of the neighbouring nodes.

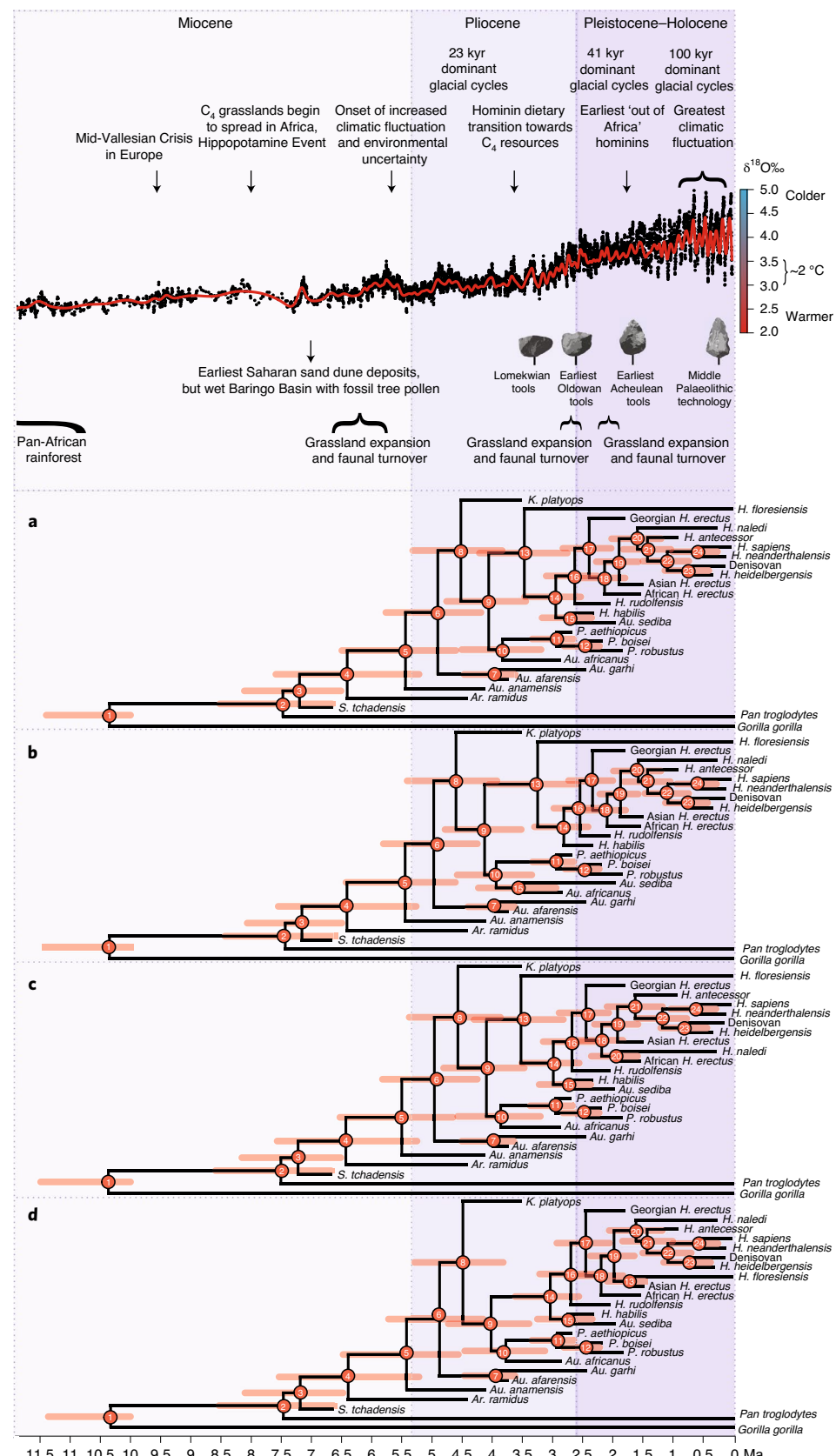


**Fig. 2 | Summary diagram of important palaeoclimatic and hominin evolution events plotted next to the four obtained consensus phylogenies and time divergence estimates. **a****, Dembo et al.<sup>17</sup> hypothesis. **b**, *Au. sediba* hypothesis. **c**, *H. naledi* hypothesis. **d**, *H. floresiensis* hypothesis. Red node bars represent the 95% HPD for the estimated node ages. A composite benthic foraminifera oxygen isotope record obtained from ref. <sup>53</sup> is displayed at the top of the figure to illustrate the evolution of high-latitude glacial cycles and dominant periodicity of glacial variability, as well as palaeotemperatures (the red line corresponds to a smoothing spline used to depict the main trend in  $\delta^{18}\text{O}$  values; smoothing parameter = 0.2).

**Table 1 | Divergence-times mean and 95% HPD in Ma for the different phylogenetic hypotheses in Fig. 1**

Node	Div. mean-d	Div. mean-s	Div. mean-n	Div. mean-f
1	10.35 (11.40, 10.00)	10.35 (11.42, 10.00)	10.37 (11.49, 10.00)	10.33 (11.36, 10.00)
2	7.47 (8.52, 6.66)	7.43 (8.43, 6.61)	7.50 (8.59, 6.67)	7.46 (8.53, 6.63)
3	7.20 (8.11, 6.51)	7.15 (8.06, 6.49)	7.22 (8.15, 6.51)	7.18 (8.10, 6.47)
4	6.40 (7.59, 5.21)	6.41 (7.55, 5.26)	6.42 (7.57, 5.24)	6.39 (7.54, 5.21)
5	5.44 (6.49, 4.60)	5.44 (6.42, 4.61)	5.50 (6.52, 4.64)	5.42 (6.47, 4.56)
6	4.90 (5.76, 4.18)	4.97 (5.80, 4.24)	4.95 (5.82, 4.24)	4.87 (5.72, 4.15)
7	3.97 (4.47, 3.63)	3.94 (4.40, 3.62)	3.98 (4.50, 3.63)	3.97 (4.46, 3.62)
8	4.52 (5.32, 3.83)	4.60 (5.41, 3.92)	4.56 (5.37, 3.86)	4.49 (5.29, 3.82)
9	4.06 (4.76, 3.44)	4.12 (4.78, 3.52)	4.09 (4.80, 3.46)	4.02 (4.73, 3.39)
10	3.83 (4.51, 3.19)	3.93 (4.58, 3.34)	3.85 (4.57, 3.19)	3.77 (4.46, 3.13)
11	2.93 (3.34, 2.65)	2.93 (3.33, 2.65)	2.94 (3.36, 2.66)	2.93 (3.34, 2.65)
12	2.47 (2.81, 2.22)	2.46 (2.79, 2.22)	2.48 (2.82, 2.22)	2.47 (2.81, 2.22)
13	3.47 (4.21, 2.75)	3.24 (4.05, 2.59)	3.52 (4.30, 2.81)	<b>1.73 (2.09, 1.47)</b>
14	2.94 (3.46, 2.53)	2.81 (3.30, 2.40)	2.98 (3.50, 2.55)	3.04 (3.62, 2.56)
15	2.70 (3.17, 2.35)	<b>3.57 (4.23, 2.94)</b>	2.73 (3.21, 2.36)	2.75 (3.25, 2.34)
16	2.63 (3.10, 2.25)	2.54 (2.97, 2.19)	2.67 (3.15, 2.28)	2.70 (3.21, 2.26)
17	2.39 (2.83, 2.02)	2.33 (2.73, 1.99)	2.44 (2.88, 2.06)	2.45 (2.93, 2.05)
18	2.13 (2.54, 1.79)	2.09 (2.47, 1.78)	2.18 (2.58, 1.82)	2.19 (2.63, 1.83)
19	1.89 (2.27, 1.57)	1.87 (2.21, 1.57)	1.91 (2.30, 1.57)	1.98 (2.37, 1.64)
20	1.59 (2.02, 1.20)	1.57 (1.99, 1.20)	<b>1.94 (2.35, 1.58)</b>	1.61 (2.06, 1.18)
21	1.42 (1.83, 1.04)	1.42 (1.81, 1.04)	1.62 (2.09, 1.17)	1.43 (1.84, 1.01)
22	1.09 (1.50, 0.73)	1.08 (1.46, 0.74)	1.17 (1.59, 0.76)	1.08 (1.50, 0.70)
23	0.77 (1.13, 0.40)	0.77 (1.12, 0.42)	0.80 (1.20, 0.43)	0.76 (1.16, 0.38)
24	0.60 (1.01, 0.26)	0.59 (0.94, 0.27)	0.63 (1.03, 0.28)	0.59 (1.02, 0.25)

The maximum and minimum bounds for the 95% HPD are in parentheses. Div. mean, divergence-times mean; d, Dembo et al.<sup>17</sup> hypothesis; s, *Au. sediba* hypothesis; n, *H. naledi* hypothesis; and f, *H. floresiensis* hypothesis. Node numbers correspond to the numbers in Fig. 2. Ages of nodes that are not comparable due to the specific changes in the phylogenetic hypotheses are indicated in bold.

Speciation events since the common ancestor of *Homo* start to occur around the mid-Pliocene at 3.3 Ma and end around the mid-Pleistocene at 0.6 Ma (Fig. 2 and Table 1). In contrast to the previous decreasing trend in body mass, the body mass ACSR show an increment from ~38 to 65 kg in this period (nodes 13/14–24; Figs. 3 and 5a–d and Extended Data Fig. 5). This corresponds to an increase in body mass of 1.71 times in 2.7 Myr, which means a reversion in body size to similar levels as the one observed at the tree's root but in less than half of the time. In other words, the rate of body mass evolution approximately doubled in the genus *Homo* from what has been previously seen (10.0 kg Myr<sup>-1</sup> versus 4.6 kg Myr<sup>-1</sup>). However, these increments were not equal in all nodes and some groups even show a body mass reduction. For instance, the parallel branch that goes from node 14 to *H. habilis* shows a decrease in body mass regardless of the position of *Au. sediba*. The effect of removing *Au. sediba* from *Homo* results in a slight increase in the reconstructed body mass at node 14. Similarly, *H. floresiensis* and *H. naledi* also displayed a considerable decrease in body mass from their ancestors in all the hypotheses. However, the decrease and its rate vary with the different hypotheses. When *H. floresiensis* is at a basal position within *Homo*, the decrease is ~10 kg (~−3.0 kg Myr<sup>-1</sup>), while when it is considered the sister taxon of the Asian *H. erectus* the decrease is ~22 kg (~−13.0 kg Myr<sup>-1</sup>). When *H. naledi* is at the stem of *H. antecessor* and its closest *Homo* relatives, the decrease is ~13 kg (~−10.1 kg Myr<sup>-1</sup>), whereas when it is the sister taxon of the African *H. erectus* the decrease is ~5 kg (~−3.0 kg Myr<sup>-1</sup>).

The PEQ ACSR for the period since the common ancestor of *Homo* (node 13/14) remains similar to the previously observed increasing trend, augmenting 1.53 times in 2.70 Myr, from ~1.88 in

node 13/14 to 2.88 in node 24 (Figs. 4 and 5e–h and Extended Data Fig. 6). Even though the increase in PEQ is similar to the PEQ evolution before the common ancestor of *Homo* (1.00 and 1.01, respectively), its rate increased 2.64 times, going from 0.14 PEQ Myr<sup>-1</sup> to 0.37 PEQ Myr<sup>-1</sup>. Within this general PEQ evolutionary trend, there are three taxa that stand out from the rest: *H. floresiensis*, *H. naledi* and *H. sapiens*, although in the first two species the specific trends vary with the different hypotheses. When *H. floresiensis* is at a basal position within *Homo*, it displays a slight decrease or stasis in PEQ from its ancestor exhibiting a value of ~1.7 for 3.4 Myr of evolutionary history, while when it is considered the sister taxon of the Asian *H. erectus* the decrease is 0.52 in 1.7 Myr (~−0.30 PEQ Myr<sup>-1</sup>). When *H. naledi* is at the stem of *H. antecessor* and its closest *Homo* relatives, the PEQ decreases ~0.85 in 1.3 Myr (~−0.65 PEQ Myr<sup>-1</sup>), whereas when it is the sister taxon of the African *H. erectus* the decrease is ~0.69 in 1.7 Myr (~−0.42 PEQ Myr<sup>-1</sup>). This strong decrease under different scenarios puts *H. naledi* very close to the PEQ values for *Au. afarensis*. In contrast, *H. sapiens* stands out due to its rapid increase in PEQ from its common ancestor with *H. neanderthalensis* (node 24), going from ~2.88 to 3.22 in ~0.55 Myr. That is 0.62 PEQ Myr<sup>-1</sup>, which is 1.68 times greater compared to the rate observed since the common ancestor of *Homo* (nodes 13/14 to 24) between 3.3 Ma and 0.6 Ma and 4.43 times greater in comparison to the rate observed since the common ancestor of *G. gorilla* and the ancestor of *Homo* (nodes 1 to 13/14) between 10.4 and 3.3 Ma.

## Discussion

We have presented TED estimates of the divergence times of most hominin taxa under different hypotheses. Our divergence estimates

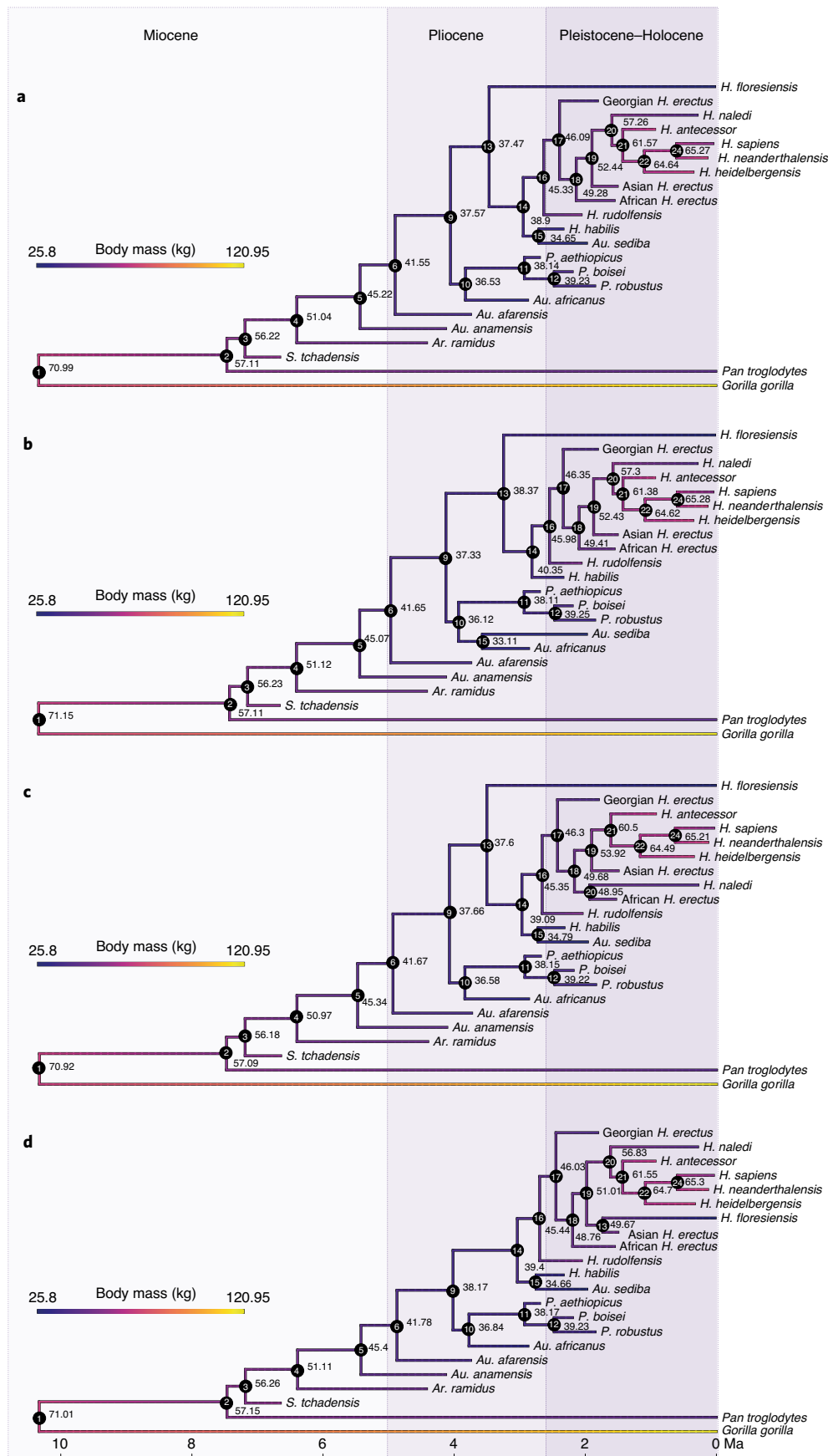


**Fig. 3 |** Body mass ACSR for each species mapped onto the four consensus time-calibrated phylogenies. **a**, Dembo et al.<sup>17</sup> hypothesis. **b**, *Au. sediba* hypothesis. **c**, *H. naledi* hypothesis. **d**, *H. floresiensis* hypothesis. The values at nodes and branches were reconstructed using an ML ancestral character estimation method under a Brownian motion model.

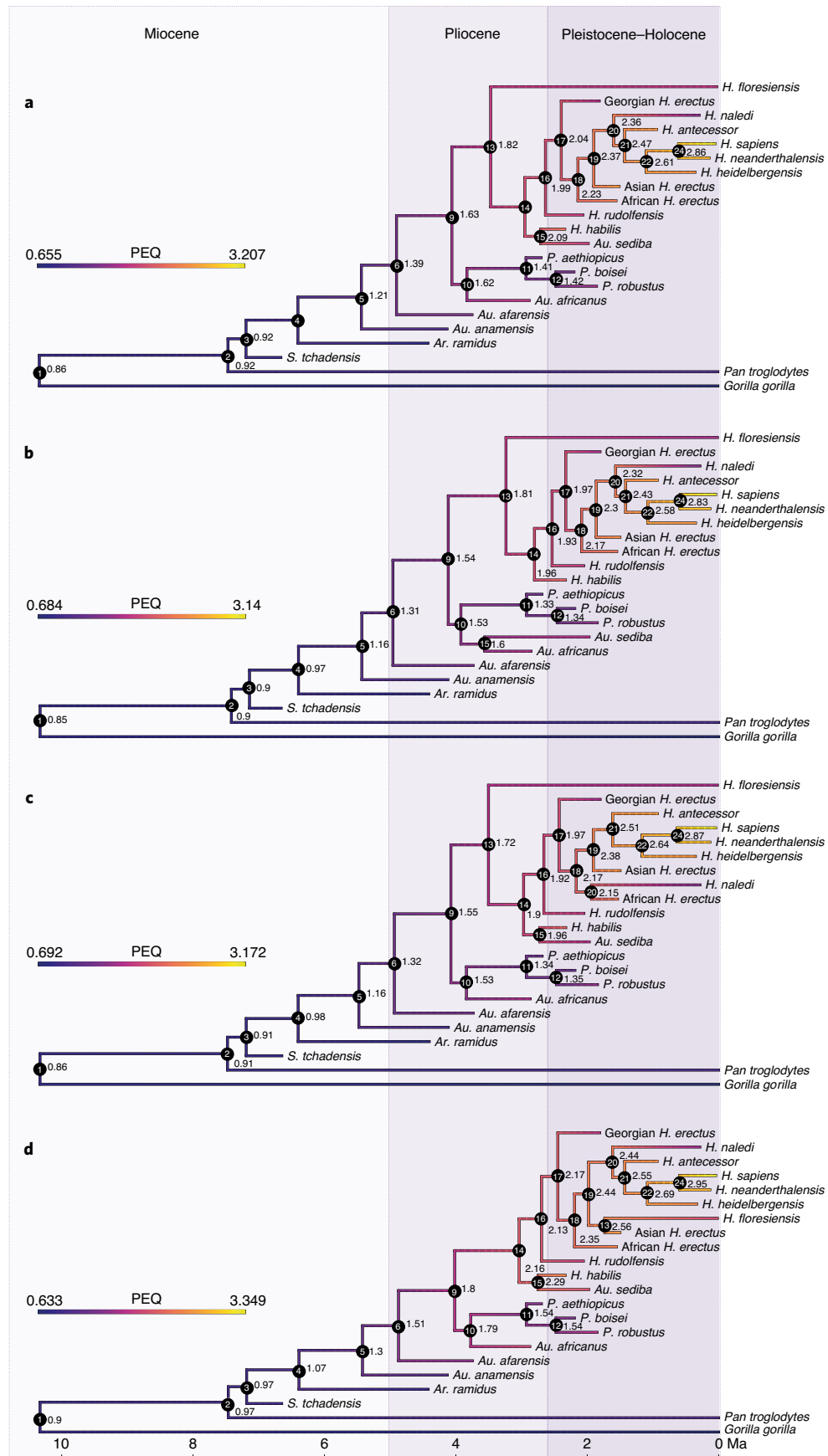


**Fig. 4 | PEQ ACSR for each species mapped onto the four consensus time-calibrated phylogenies.** **a**, Dembo et al.<sup>17</sup> hypothesis. **b**, *Au. sediba* hypothesis. **c**, *H. naledi* hypothesis. **d**, *H. floresiensis* hypothesis. The values at nodes and branches were reconstructed using an ML ancestral character estimation method under a Brownian motion model.

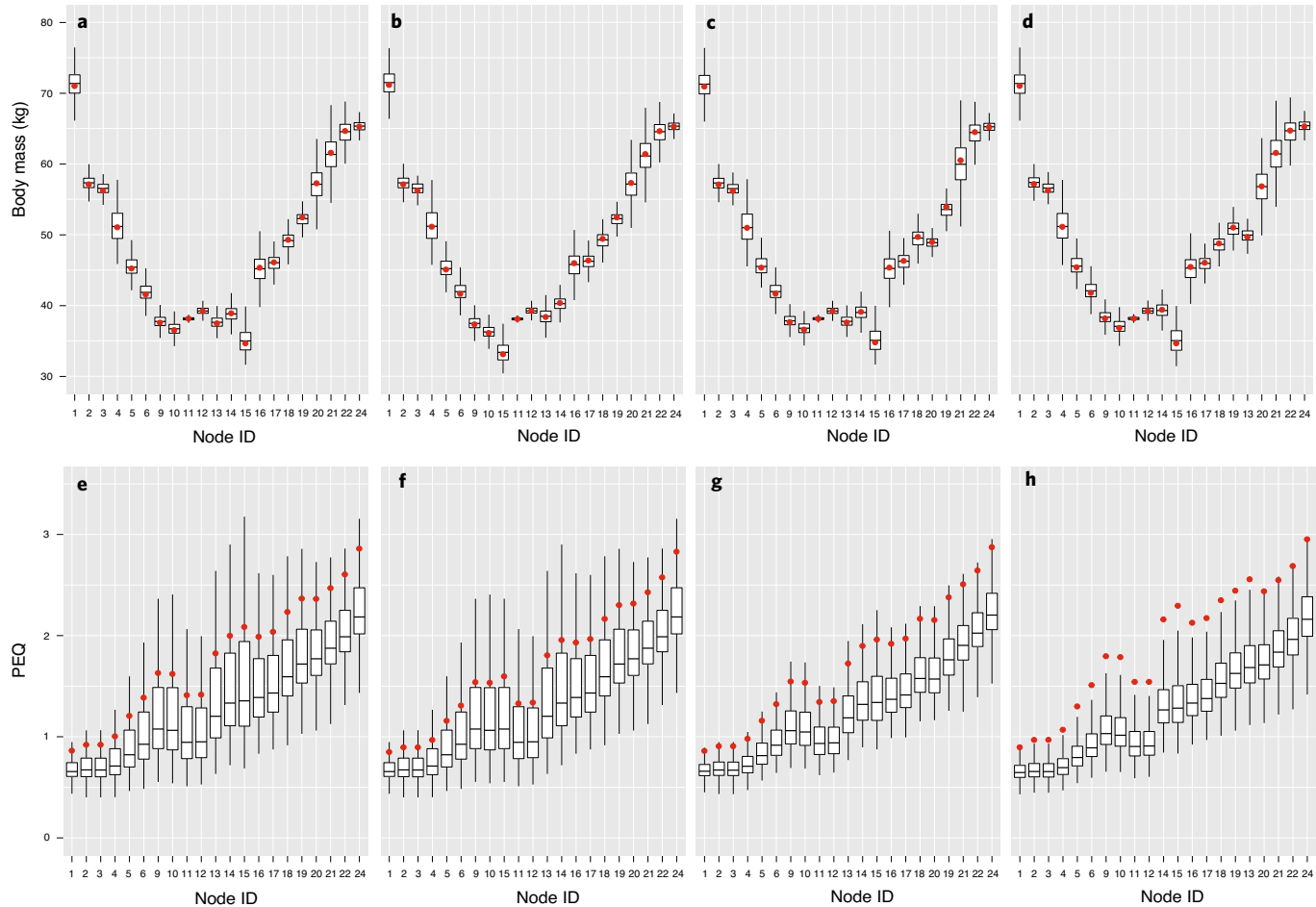


**Fig. 5 | Boxplots of body mass (kg) and PEQ ACSR per node on the basis of a sample of 9,002 time-calibrated posterior trees.** **a-d**, Body mass (kg): Dembo et al.<sup>17</sup> hypothesis (**a**); *Au. sediba* hypothesis (**b**); *H. naledi* hypothesis (**c**); *H. florensis* hypothesis (**d**). **e-h**, PEQ: Dembo et al.<sup>17</sup> hypothesis (**e**); *Au. sediba* hypothesis (**f**); *H. naledi* hypothesis (**g**); *H. florensis* hypothesis (**h**). The red dots indicate the ACSR conducted using the consensus trees. The median is indicated by the horizontal black line, the interquartile range (IQR) is the white box and the whiskers indicate the minimum and the maximum (at 1.5 × IQR of the lower- and upper-hinge, respectively).

are in general agreement with previous molecular studies using fossil node-calibrations<sup>30–34</sup>, as well as with fossil calibration independent methods, such as those using generation times<sup>35</sup>. The topology of our trees (Fig. 2) differs from the trees of Dembo et al.<sup>16,17</sup> in the position of *H. neanderthalensis* relative to *H. sapiens* and *H. heidelbergensis*, which is probably due to the influence of the mitochondrial DNA (mtDNA) in our total evidence analysis. The position of these groups plus Denisovans is the same as obtained in a previous study<sup>34</sup> using mtDNA but differs from studies using nuclear DNA<sup>36</sup>, probably related to an mtDNA introgression event that occurred ~270 thousand years ago (ka) (ref. <sup>37</sup>). We think our divergence-time estimates are robust and consistent with the current evidence available. However, further refinements in some of the fossilized birth-death (FBD) model's assumptions, namely being able to consider a non-uniform fossil sampling among clades<sup>38</sup> and new fossil discoveries, could further improve these estimates.

Our ACSR results from the four different considered hypotheses are consistent between them, showing that refining the phylogenetic affinities of problematic taxa (for example, *H. naledi*) would probably have a minor impact in major body size and encephalization trends in hominin evolution. Furthermore, our ACSR results are consistent with previous studies that show that body size in hominins has not been a simple linear increment since the divergence with *P. troglodytes*<sup>26,27,39</sup>. The observed decreasing trend in body

size from the root of the tree is in agreement with previous studies that suggest a chimpanzee-sized common ancestor with *P. troglodytes*<sup>40,41</sup>. Our ACSR results also displayed a general trend towards greater body size that started after the emergence of the last common ancestor of *Homo*, contrary to a previous claim stating that there were no clear body mass temporal trends in hominin evolution<sup>26</sup>. Instead, our results showed a complex history of body size changes that do not correlate linearly with brain size changes. It may be that after the emergence of the genus *Homo*, brain size carried body size increases as previously suggested<sup>42</sup> (Extended Data Fig. 10i–l). However, before the emergence of *Homo*, brain size and body size seem to be decoupled or following opposite directions (Extended Data Fig. 10e–h). Our results also agree with Pagel's<sup>43</sup> seminal work and other studies (for example, refs. <sup>44–46</sup>) that showed a general trend of gradual but accelerating brain size evolution in hominins. However, some of them (refs. <sup>44,45</sup>) directly analysed endocranial volume (ECV) without taking into account body mass estimations, which we considered in our PEQ estimations. This is problematic because it is only when body size is taken into account<sup>47</sup> and phylogeny is included that we can consider whether observed brain size differences are meaningful in terms of encephalization<sup>28,48,49</sup>. We are confident that our ACSR are reliable and consistent with the current evidence. Nevertheless, it is important to note that the inclusion of more fossils near the root could have an impact in the ACSR, in

particular for the oldest nodes of the tree. Additionally, ACSR could be affected by the use of different methods and models of character evolution<sup>50</sup>.

That PEQ evolution tends to accelerate when moving from a relatively stable climate to more unstable climatic conditions (Fig. 2) appears to agree with the ‘variability selection’ hypothesis which correlates major adaptations in hominins with periods of high climatic variability<sup>51,52</sup>. Before the emergence of *Homo*, hominin evolution occurred in a mostly warm period although with a global cooling trend, which had started after the Mid-Miocene Climatic Optimum and the recovery of Antarctic ice-sheets ~10 Ma (ref. <sup>53</sup>). From a common ancestor with *P. troglodytes* at ~7.5 Ma, bipedalism started to emerge at least by 6 Ma (refs. <sup>54–57</sup>) in the hominin lineage. This relatively stable period was interrupted by considerable temperature oscillations around the Miocene/Pliocene boundary at 5.3 Ma. Subsequently with the development of 23-kyr dominant glacial cycles, we observed the emergence of the genus *Homo* and an evolutionary shift, displaying the end of a general trend towards smaller body size and the beginning of an acceleration of the increase in PEQ and the start of a general trend towards larger body masses (Figs. 2–4). Even though the earliest member of *Homo* discovered so far was from 2.8 Ma (ref. <sup>58</sup>), our analysis allows us to predict the presence of early representatives of the *Homo* lineage not yet found (or identified) in the African fossil record ~3.3 Ma (0.5 Myr earlier). Interestingly, 3.3 Ma is the age attributed to stone tools discovered in West Turkana<sup>59</sup>, which are commonly associated with *K. platyops*<sup>60</sup> and *Au. afarensis*<sup>61</sup>.

After the Pliocene/Pleistocene boundary at 2.58 Ma, the trend towards cooler temperatures and aridity continues and 41-kyr dominant glacial cycles are established, with an intensification of climatic fluctuations. As PEQ continues to increase, so does the evidence of increasingly complex behaviours: tool innovations (Oldowan (2.6 Ma; ref. <sup>62</sup>), Acheulean (1.7–1.4 Ma; ref. <sup>63</sup>) and Aurignacian at (120–~50 ka; ref. <sup>64</sup>)), the use of fire (from 1.5 Ma onwards<sup>65,66</sup> (strong evidence at 1.0–0.5 Ma; ref. <sup>67</sup>)), cooking and more frequent meat consumption<sup>68–70</sup> and the ability to produce art at ~540–430 ka (ref. <sup>71</sup>). By 300 ka, Africa was inhabited by at least three *Homo* species, *H. sapiens*, *H. heidelbergensis* and *H. naledi* and Eurasia by *H. neanderthalensis*, Denisovans, *H. floresiensis*, *H. luzzonensis* and also possibly *H. erectus* and *H. heidelbergensis*<sup>72</sup>. *Homo sapiens* is the hominin species with the highest PEQ, so a possible explanation for its exclusive continuation would be that this difference in PEQ allowed *H. sapiens* to outcompete its contemporary relatives<sup>47,73–75</sup>. Even though it has been recently established that there was not a unique ‘Out of Africa’ event in *H. sapiens* history<sup>76–79</sup>, it is widely accepted that Neanderthals were eventually displaced by *H. sapiens* in Europe by ~39 ka (ref. <sup>80</sup>). However, it is now understood that *H. neanderthalensis* was capable of very complex human behaviours<sup>81,82</sup>.

Like *H. sapiens*, *H. neanderthalensis* was certainly a cultural niche constructor<sup>83–85</sup> under harsh glacial–interglacial temperature fluctuations<sup>86</sup>. Nonetheless, *H. sapiens* not only displays a higher PEQ but also a higher rate of change in PEQ compared to *H. neanderthalensis*. This probably means that within Hominini, PEQ selection was particularly strong within and between the metapopulations of *H. sapiens*<sup>87</sup> in an arid–moist fluctuating Africa<sup>86</sup>. A larger relative brain mass has been associated in mammals with behavioural flexibility, adaptation and resilience in variable environmental conditions<sup>88</sup>. Therefore, in spite of the fact that the behavioural gap between the two species may have been minimal, even a small advantage in terms of behavioural flexibility and ability to adjust in a variable environment as it was during the late Pleistocene<sup>89</sup>, could have had enormous benefits in terms of fitness and successful competition for *H. sapiens*<sup>90,91</sup>. A similar explanation could also be applied for the demise of the rest of our contemporaneous relatives exhibiting an even lower PEQ.

Considering the evolution of *H. floresiensis*, it seems that selection was acting on body size by means of heterochrony<sup>92,93</sup> favouring a reduction in body size as a mean of decreasing the energetic expenditure in a small island environment with limited resources as it also probably occurred for *Stegodon florensis*<sup>94–96</sup>. However, our results show that resolving the phylogenetic affinities of *H. floresiensis* would have important implications for the evolutionary trends on this taxon. The body size reduction in *H. floresiensis* is more spectacular if this taxon derives or is considered closely related to Asian *H. erectus*<sup>97</sup>, a scenario that also implies a notorious encephalization reduction. Nevertheless, more recent studies favour *H. floresiensis* at a basal position within *Homo*<sup>16,17,98</sup>, which would then favour a encephalization stasis scenario. Interestingly, if tool development can be associated with a certain level of cognition, considering the tools attributed to *H. floresiensis*<sup>99,100</sup>, we anticipate that the common ancestor of *Homo* with a similar PEQ value, was most likely able to make stone tools as well.

Previous studies have described *H. naledi* as a small-bodied and small-brained hominin of the genus *Homo*<sup>101</sup>, with cranial<sup>102</sup>, endocranial<sup>103</sup> and postcranial features<sup>104,105</sup> that support this placement. There are two hypotheses which attempt to explain this small brain as either a (1) retention from the common ancestor from the genus *Homo* or (2) a reduction from a later big-brained form of *Homo*<sup>103</sup>. The PEQ trends displayed by *H. naledi*’s ACSR supports the second hypothesis because there is an extraordinary reduction in PEQ from a big-brained ancestor in a relatively short time, although this reduction is faster if *H. naledi* is at the stem of *H. antecessor* and its closest *Homo* relatives as previously suggested<sup>17</sup>. *Homo naledi* lived between 236 and 335 ka (ref. <sup>106</sup>) in South Africa, with a PEQ of ~1.5, which is really close to *Au. afarensis* and other australopiths. This happened at a time in which big-bodied and big-brained hominins were the norm in continental landmasses, like *H. sapiens* and *H. neanderthalensis* both with a PEQ >2.7. Even the insular small-sized *H. floresiensis* had a higher PEQ. In a context of increasing PEQ over the hominin lineage at that time, the PEQ reduction in *H. naledi* could perhaps be explained, by the specialization in a niche of scarce and/or low energy food resources in which an expensive large brain would be prejudicial. Hypotheses in relation to the cost of encephalization like the ‘expensive tissue’<sup>107,108</sup> and the ‘energy trade off’ hypotheses<sup>109</sup>, could potentially explain this trend in *H. naledi*. Less energy expenditure could also explain the considerable body size reduction observed in *H. naledi* from its reconstructed bigger-brained ancestors. In fact, through dental topography comparisons it has been suggested that *H. naledi* was occupying a distinct ecological niche, which was different from previous and contemporaneous hominins<sup>110</sup>.

In conclusion, our TED analyses and ACSR results showed that (1) the last common ancestor of the genus *Homo* probably appeared around 3.3 Ma (4.30–2.56 Ma) with a body size close to that of *Au. afarensis* and an encephalization very similar to *H. floresiensis*, (2) hominin body mass evolution followed a general decreasing trend before the emergence of *Homo* and exhibited a general increasing trend afterwards and (3) hominins displayed a general trend of gradual but accelerating encephalization through time.

## Methods

**Data collection and TED analyses.** We used TED analyses which are a collection of Bayesian phylogenetic methods (see ref. <sup>111</sup> for a general primer and refs. <sup>19,20,22,112,113</sup> for reviews of Bayesian molecular dating methodology). For the TED analysis, our taxon sampling was similar to previous published analyses<sup>17</sup> but Denisovans were also included. The morphological data were obtained from the same study<sup>17</sup> and comprised a supermatrix of 391 craniodental characters from matrices used in 13 previous studies<sup>14–126</sup>. Even though there are more recently published hominin phylogenetic analyses computed using different morphological matrices<sup>127,128</sup>, the morphological matrix used here<sup>17</sup> includes more character states and hominin species.

The molecular data were complete mtDNA genomes extracted from GenBank for the species for which it was available: *G. gorilla* (KF914214.1), *P. troglodytes*

(JF727180.2), *H. heidelbergensis* (KF683087.1), *H. neanderthalensis* (MK123269.1), *H. sapiens* (KC417443.1) and Denisovans (KX663333.1). Following previous analyses<sup>34,129</sup>, we removed the D-loop region from the mtDNA due to the differential rate at which it acquires substitutions. We aligned the sequences with the MUSCLE algorithm in MEGA X (ref. <sup>130</sup>). Then, we analysed the alignment using PartitionFinder2 (ref. <sup>131</sup>) using the ‘greedy’ algorithm<sup>132</sup>, to select the most appropriate models of molecular evolution for the different protein coding and non-coding regions of the mtDNA. The best partitioning scheme on the basis of corrected Akaike information criterion score included 16 partitions for the mtDNA (Supplementary Table 1). We used these partitions for the mtDNA sequences and the Mkv +  $\Gamma$  model<sup>133</sup> for the morphological data, unlinking the model parameters across these partitions. To avoid a mismatch in our model, we used the dates associated with our data following the recommended procedure<sup>34</sup>, which meant that we did not necessarily calibrate a tip using the oldest or first fossil occurrence for a particular taxon. Hence, we calibrated the fossil tips of the tree using the age of the fossil specimen used for scoring morphology in taxa without mtDNA available. In taxa with mtDNA sequences available, the sequences were selected from individuals aged equally, or as close as possible, to the morphologically scored fossils and the age associated with these sequences was used to calibrate the fossil tips. We also considered radiometric age uncertainties using a uniform distribution between the maximum and minimum estimated ages for each fossil when available<sup>12</sup> (Supplementary Table 2).

The selected outgroup was *G. gorilla* and the root of the tree was calibrated using a uniform distribution between 10.00 and 12.5 Ma. The minimum age of 10 Ma and the maximum age of 12.5 Ma were based on the appearance of the proposed stem member of the gorilla clade *Nakalipithecus nakayamai*<sup>135,136</sup> and the probable crown pongine *Sivapithecus*<sup>137,138</sup>, respectively. Even though there is uncertainty regarding the exact phylogenetic placement of *N. nakayamai*<sup>135,136</sup>, we consider that the anatomical features linking it with gorillas are strong enough to use the age associated with this taxon as minimum divergence date for hominines, particularly when considering the possible ancestral–descendent relationship between *N. nakayamai* and the basal gorillin *Chororapithacus abyssinicus*<sup>135,139,140</sup>.

We used a normally distributed clock rate prior, with a mean of 0.025 and standard deviation of 0.05, which is consistent with previous estimates of the mitochondrial rate of evolution in humans<sup>141,142</sup>. The independent gamma rate relaxed clock model was used for modelling branch rate variation, using a clock rate variance prior with an exponential distribution of rate 10. We used the FBD model as the prior on divergence times, using an exponential net diversification prior with rate 1, a beta turnover prior with shape parameters  $\alpha=1$  and  $\beta=1$ , a beta fossil sampling proportion prior with shape parameters  $\alpha=1$  and  $\beta=1$  and an extant sampling proportion of 1. The priors used in clock rate variance and the FBD model were intentionally diffuse, reflecting the general uncertainty in our prior expectation of the distribution of these parameters.

Even though our main focus was estimating hominin divergence times, we are aware that there is still controversy regarding the phylogenetic placement of some of the taxa included in our matrix, particularly in the placement of *Au. sediba*<sup>117</sup>, *H. florensiensis*<sup>16,97,98</sup> and *H. naledi*<sup>17,143</sup>. Therefore, we considered four different topological hypotheses for constraining four independent phylogenetic analyses (Fig. 1): a topology similar to the phylogeny of the analysis from which we extracted the morphological data (Fig. 1a)<sup>17</sup>; the same topology as Fig. 1a but moving *Au. sediba* from the *Homo* clade to be the sister taxon of *Au. africanus* as it has been recently suggested (Fig. 1b)<sup>144</sup>; the same topology as Fig. 1a but changing the position of *H. naledi* from the stem of *Homo antecessor* and its closest *Homo* relatives to be the sister taxon of the African *H. erectus* as previously suggested (Fig. 1c)<sup>143,145</sup>; and the same topology as Fig. 1a but taking *H. florensiensis* from its basal position within the genus *Homo* to be the sister taxon of the Asian *H. erectus* as it was originally suggested (Fig. 1d)<sup>97</sup>. Nevertheless, we left *H. sapiens*, *H. neanderthalensis*, *H. heidelbergensis* and Denisovans unconstrained in the four analyses as they had mtDNA sequences which could also be informative of their phylogenetic relationships. Therefore, the constraints we used in all the analyses were soft, so the latter taxa could be accommodated in any position of the tree according to their morphological, molecular and stratigraphic information.

We performed the analyses with MrBayes 3.2.7a (ref. <sup>146</sup>) using two runs of four chains and 60 million Markov chain Monte Carlo (MCMC) generations with the first 25% of samples discarded as burn-in. The analyses were run on CIPRES portal v.3.3 (ref. <sup>147</sup>). We ensured that the average standard deviation of split frequencies was  $<0.01$  and that all parameters had an effective sample size of  $>200$ . Additionally, we visually inspected that the two independent runs achieved convergence and stationarity using the program Tracer v.1.7.1 (ref. <sup>148</sup>).

**Evaluating the prior sensitivity of divergence-time estimates.** To evaluate the effect of alternative priors on our divergence-time estimates, we conducted sensitivity analyses in the first tree (Dembo et al.<sup>17</sup> hypothesis) in which we changed the prior distribution of one important model parameter at a time into a reasonable alternative prior distribution, keeping the rest of the model parameters unchanged. This was done for the clock rate variance, the net diversification prior of the FBD model and root age prior. We did this in the former two cases because we wanted to test the effect of using more constrained priors and, in the latter, to account for the possibility that *N. nakayamai* could be a stem hominin before

the gorilla–human split<sup>135,136</sup>. Therefore, for the clock rate variance prior, we ran a strict clock and a non-clock analysis constrained to have the same topology. Then, following the methodology of Ronquist et al.<sup>25</sup> to estimate rate variance, the clock rate variance prior was estimated as 25.04. For the net diversification prior we followed Zhang et al.<sup>149</sup> in using an exponential distribution of rate 100. In the case of the root age prior we used a uniform distribution changing the minimum to 8 Ma but keeping the maximum in 12.5 Ma, because of the 8 Ma estimated for appearance of the proposed gorillin *C. abyssinicus*<sup>135,139</sup>, which have been used to date the minimum age of the gorilla–human split in previous studies<sup>32,33</sup>.

**Estimating PEQ using a PGLS regression.** The encephalization quotient (EQ) is commonly used to determine how brain size scales with respect to body size for a given individual<sup>48,150–152</sup>. However, EQ does not take into account phylogenetic information, so a newly proposed measurement termed PEQ has been advanced as a way of considering the phylogenetic non-independence between data points<sup>28</sup>.

Body mass and ECV were obtained from the literature (Supplementary Table 3). When more than one specimen was available, arithmetic averages for body mass and ECV were used. ECV was converted into brain mass by dividing by 1.036 (ref. <sup>153</sup>). We used R v.3.6.1 (ref. <sup>154</sup>) and the packages ‘ape’<sup>155</sup> and ‘nlme’<sup>156</sup> to compute phylogenetic correlations and to fit linear models, respectively. We log-scaled the data and, by assuming a Brownian motion model of evolution we calculated a correlation using the corBrownian() function to then fit a linear model (brain mass was the dependent variable, whilst body mass was the independent one) independently for each one of the four consensus trees obtained in the TED analysis (Extended Data Fig. 8).  $R^2$  were calculated using the R package rr2 v.1.0.2 and the function R2.pred() (ref. <sup>157</sup>). The resulting equations were used to calculate the expected brain mass (E) and PEQ was calculated as the ratio between the actual estimated brain mass (A) and E ( $PEQ = A/E$ ) for each one of the living and fossil taxa (Supplementary Table 3).

**PEQ and body mass ancestral character state reconstructions.** We used an ML approach to perform the ACSR at the internal nodes of the four consensus phylogenetic trees for (1) body mass and (2) PEQ (and brain mass) under a Brownian motion model. This procedure was performed using the fastAnc() and the contMap() functions from the package ‘phytools’ v.0.6-99 (ref. <sup>158</sup>). *Kenyanthropus platyops* and *Au. garhi* tips were dropped from the ACSR for body mass and PEQ as there are no available body mass estimations for these taxa due to their fragmentary fossil record. Similarly, Denisovans were removed from all ACSR analyses as there are no available estimates for their brain and body mass.

**Measuring uncertainty in the ML ancestral character state reconstructions.** To measure the uncertainty in our ML ACSR we sampled every tenth time-calibrated tree from the posterior after discarding the first 25% as burn-in, which meant a total of 9,002 time-calibrated posterior trees sampled for each one of the four analyses. Then we ran ML ACSR analyses in all of these trees and their internal nodes for (1) body mass and (2) PEQ (and brain mass), using the same methods and R packages described in the previous section. For the PEQ ACSR, we previously ran the PGLS analysis for each one of the sampled trees, so the PEQ values in the trees’ tips were independently estimated for each tree. This allowed us to incorporate uncertainty in our ACSR and to analyse if the patterns observed in the ACSR for the consensus trees held or not when we looked at different trees recovered from the posterior.

**Measuring the relationship between ACSR of brain mass and body mass.** As brain size increase has been proposed as a driver of body size increase<sup>42</sup>, we carried out regressions between our ACSR of brain mass versus body mass in the four consensus trees to test if there was a pattern that could be consistent with that hypothesis. It is important to consider that we did not directly assess whether brain size increase drove body mass evolution but rather evaluate if there was a general pattern that could provide further information about this issue. Both ACSR datasets were log-scaled before performing the regressions.

**Reporting Summary.** Further information on research design is available in the Nature Research Reporting Summary linked to this article.

## Data availability

All data analysed in this study are available in Supplementary Tables 2 and 3 and in a permanent repository at <https://doi.org/10.5281/zenodo.4537445>. Additionally, the data are available in an open access repository at <https://github.com/HansPueschel/Hominin-div-time-evolution>.

## Code availability

The code and input files are available in a permanent repository at <https://doi.org/10.5281/zenodo.4537445>. In addition, the code and input files are available in an open access repository at <https://github.com/HansPueschel/Hominin-div-time-evolution>.

Received: 5 May 2020; Accepted: 25 February 2021;  
Published online: 01 April 2021

## References

1. Du, A. & Alemseged, Z. Temporal evidence shows *Australopithecus sediba* is unlikely to be the ancestor of *Homo*. *Sci. Adv.* **5**, eaav9038 (2019).
2. Du, A., Rowan, J., Wang, S. C., Wood, B. A. & Alemseged, Z. Statistical estimates of hominin origination and extinction dates: a case study examining the *Australopithecus anamensis–afarensis* lineage. *J. Hum. Evol.* **138**, 102688 (2020).
3. Finarelli, J. A. & Clyde, W. C. Reassessing hominoid phylogeny: evaluating congruence in the morphological and temporal data. *Paleobiology* **30**, 614–651 (2004).
4. DeMenocal, P. B. African climate change and faunal evolution during the Pliocene–Pleistocene. *Earth Planet. Sci. Lett.* **220**, 3–24 (2004).
5. DeMenocal, P. B. Climate and human evolution. *Science* **331**, 540–542 (2011).
6. Antón, S. C. & Josh Snodgrass, J. Origins and evolution of genus *Homo*: new perspectives. *Curr. Anthropol.* **53**, S479–S496 (2012).
7. Harcourt-Smith, W. E. H. Early hominin diversity and the emergence of the genus *Homo*. *J. Anthropol. Sci.* **94**, 19–27 (2016).
8. Villmoare, B. Early *Homo* and the role of the genus in paleoanthropology. *Am. J. Phys. Anthropol.* **165**, 72–89 (2018).
9. de Ruiter, D. J., Churchill, S. E., Hawks, J. & Berger, L. R. Late australopiths and the emergence of *Homo*. *Annu. Rev. Anthropol.* **46**, 99–115 (2017).
10. Skelton, R. R. & McHenry, H. M. Evolutionary relationships among early hominids. *J. Hum. Evol.* **23**, 309–349 (1992).
11. Strait, D. S., Grine, F. E. & Moniz, M. A. A reappraisal of early hominid phylogeny. *J. Hum. Evol.* **32**, 17–82 (1997).
12. Smith, H. F. & Grine, F. E. Cladistic analysis of early *Homo* crania from Swartkrans and Sterkfontein, South Africa. *J. Hum. Evol.* **54**, 684–704 (2008).
13. Bobe, R. & Leakey, M. G. in *The First Humans: Origins of the Genus Homo* (eds Grine, F. E. et al.) 173–184 (Springer, 2009); [https://doi.org/10.1007/978-1-4020-9980-9\\_15](https://doi.org/10.1007/978-1-4020-9980-9_15)
14. Bobe, R. & Carvalho, S. Hominin diversity and high environmental variability in the Okote Member, Koobi Fora Formation, Kenya. *J. Hum. Evol.* **126**, 91–105 (2019).
15. Maxwell, S. J. *The Quality of the Early Hominin Fossil Record: Implications for Evolutionary Analyses*. PhD thesis, Univ. College London (2018).
16. Dembo, M., Matzke, N. J., Mooers, A. & Collard, M. Bayesian analysis of a morphological supermatrix sheds light on controversial fossil hominin relationships. *Proc. R. Soc. B* **282**, 20150943 (2015).
17. Dembo, M. et al. The evolutionary relationships and age of *Homo naledi*: an assessment using dated Bayesian phylogenetic methods. *J. Hum. Evol.* **97**, 17–26 (2016).
18. Donoghue, P. C. J. & Benton, M. J. Rocks and clocks: calibrating the Tree of Life using fossils and molecules. *Trends Ecol. Evol.* **22**, 424–431 (2007).
19. Donoghue, P. C. J. & Yang, Z. The evolution of methods for establishing evolutionary timescales. *Philos. Trans. R. Soc. B* **371**, 20160020 (2016).
20. Dos Reis, M., Donoghue, P. C. J. & Yang, Z. Bayesian molecular clock dating of species divergences in the genomics era. *Nat. Rev. Genet.* **17**, 71–80 (2016).
21. Kumar, S. & Blair Hedges, S. Advances in time estimation methods for molecular data. *Mol. Biol. Evol.* **33**, 863–869 (2016).
22. Bromham, L. et al. Bayesian molecular dating: opening up the black box. *Biol. Rev.* **93**, 1165–1191 (2017).
23. Ronquist, F., Lartillot, N. & Phillips, M. J. Closing the gap between rocks and clocks using total-evidence dating. *Philos. Trans. R. Soc. B* **371**, 20150136 (2016).
24. Pyron, R. A. Divergence time estimation using fossils as terminal taxa and the origins of lissamphibia. *Syst. Biol.* **60**, 466–481 (2011).
25. Ronquist, F. et al. A total-evidence approach to dating with fossils, applied to the early radiation of the Hymenoptera. *Syst. Biol.* **61**, 973–999 (2012).
26. Grabowski, M., Hatala, K. G., Jungers, W. L. & Richmond, B. G. Body mass estimates of hominin fossils and the evolution of human body size. *J. Hum. Evol.* **85**, 75–93 (2015).
27. Jungers, W. L., Grabowski, M., Hatala, K. G. & Richmond, B. G. The evolution of body size and shape in the human career. *Philos. Trans. R. Soc. B* **371**, 20150247 (2016).
28. Ni, X., Flynn, J. J., Wyss, A. R. & Zhang, C. Cranial endocast of a stem platyrhine primate and ancestral brain conditions in anthropoids. *Sci. Adv.* **5**, eaav7913 (2019).
29. Melchionna, M. & Mondanaro, A. Macroevolutionary trends of brain mass in primates. *Biol. J. Linn. Soc.* **129**, 14–25 (2020).
30. Chatterjee, H. J., Ho, S. Y., Barnes, I. & Groves, C. Estimating the phylogeny and divergence times of primates using a supermatrix approach. *BMC Evol. Biol.* **9**, 259 (2009).
31. Dos Reis, M. et al. Phylogenomic datasets provide both precision and accuracy in estimating the timescale of placental mammal phylogeny. *Proc. R. Soc. B* **279**, 3491–3500 (2012).
32. Dos Reis, M. et al. Using phylogenomic data to explore the effects of relaxed clocks and calibration strategies on divergence time estimation: primates as a test case. *Syst. Biol.* **67**, 594–615 (2018).
33. Pozzi, L. et al. Primate phylogenetic relationships and divergence dates inferred from complete mitochondrial genomes. *Mol. Phylogenet. Evol.* **75**, 165–183 (2014).
34. Meyer, M. et al. A mitochondrial genome sequence of a hominin from Sima de los Huesos. *Nature* **505**, 403–406 (2014).
35. Langergraber, K. E. et al. Generation times in wild chimpanzees and gorillas suggest earlier divergence times in great ape and human evolution. *Proc. Natl. Acad. Sci. USA* **109**, 15716–15721 (2012).
36. Meyer, M. et al. Nuclear DNA sequences from the Middle Pleistocene Sima de los Huesos hominins. *Nature* **531**, 504–507 (2016).
37. Posth, C. et al. Deeply divergent archaic mitochondrial genome provides lower time boundary for African gene flow into Neanderthals. *Nat. Commun.* **8**, 16046 (2017).
38. Gavryushkina, A. & Zhang, C. in *The Molecular Evolutionary Clock: Theory and Practice* (ed. Ho, S. Y. W.) 175–193 (Springer International, 2020); [https://doi.org/10.1007/978-3-030-60181-2\\_11](https://doi.org/10.1007/978-3-030-60181-2_11)
39. Will, M., Pablos, A. & Stock, J. T. Long-term patterns of body mass and stature evolution within the hominin lineage. *R. Soc. Open Sci.* **4**, 171339 (2017).
40. Grabowski, M. & Jungers, W. L. Evidence of a chimpanzee-sized ancestor of humans but a gibbon-sized ancestor of apes. *Nat. Commun.* **8**, 880 (2017).
41. Grabowski, M., Hatala, K. G. & Jungers, W. L. Body mass estimates of the earliest possible hominins and implications for the last common ancestor. *J. Hum. Evol.* **122**, 84–92 (2018).
42. Grabowski, M. Bigger brains led to bigger bodies?: the correlated evolution of human brain and body size. *Curr. Anthropol.* **57**, 174–196 (2016).
43. Pagel, M. in *Morphology, Shape and Phylogeny* (eds MacLeod, N. & Forey, P. L.) 269–286 (Taylor and Francis, 2002); <https://doi.org/10.1201/9780203165171>
44. Gómez-Robles, A., Smaers, J. B., Holloway, R. L., Polly, P. D. & Wood, B. A. Brain enlargement and dental reduction were not linked in hominin evolution. *Proc. Natl. Acad. Sci. USA* **114**, 468–473 (2017).
45. Diniz-Filho, J. A. F., Jardim, L., Mondanaro, A. & Raia, P. Multiple components of phylogenetic non-stationarity in the evolution of brain size in fossil hominins. *Evol. Biol.* **46**, 47–59 (2019).
46. Miller, I. F., Barton, R. A. & Nunn, C. L. Quantitative uniqueness of human brain evolution revealed through phylogenetic comparative analysis. *eLife* **8**, e41250 (2019).
47. McHenry, H. M. & Coffing, K. *Australopithecus* to *Homo*: transformations in body and mind. *Annu. Rev. Anthropol.* **29**, 125–146 (2000).
48. Grabowski, M., Vojcik, K. L. & Hansen, T. F. Evolutionary modeling and correcting for observation error support a 3/5 brain–body allometry for primates. *J. Hum. Evol.* **94**, 106–116 (2016).
49. Montgomery, S. H., Capellini, I., Barton, R. A. & Mundy, N. I. Reconstructing the ups and downs of primate brain evolution: implications for adaptive hypotheses and *Homo floresiensis*. *BMC Biol.* **8**, 9 (2010).
50. Castiglione, S. et al. Ancestral state estimation with phylogenetic ridge regression. *Evol. Biol.* **47**, 220–232 (2020).
51. Potts, R. Environmental hypotheses of hominin evolution. *Am. J. Phys. Anthropol.* **107**, 93–136 (1998).
52. Potts, R. Evolution and climate variability. *Science* **273**, 922–923 (1996).
53. Zachos, J., Pagani, H., Sloan, L., Thomas, E. & Billups, K. Trends, rhythms, and aberrations in global climate 65 Ma to present. *Science* **292**, 686–693 (2001).
54. Richmond, B. G. & Jungers, W. L. *Orrorin tugenensis* femoral morphology and the evolution of hominin bipedalism. *Science* **319**, 1662–1665 (2008).
55. Crompton, R. H., Vereecke, E. E. & Thorpe, S. K. S. Locomotion and posture from the common hominoid ancestor to fully modern hominins, with special reference to the last common panin/hominin ancestor. *J. Anat.* **212**, 501–543 (2008).
56. Almécija, S. et al. The femur of *Orrorin tugenensis* exhibits morphometric affinities with both Miocene apes and later hominins. *Nat. Commun.* **4**, 2888 (2013).
57. Kuperavage, A., Pokrajac, D., Chavanaves, S. & Eckhardt, R. B. Earliest known hominin calcar femorale in *Orrorin tugenensis* provides further internal anatomical evidence for origin of human bipedal locomotion. *Anat. Rec.* **301**, 1834–1839 (2018).
58. Villmoare, B. et al. Early *Homo* at 2.8 Ma from Ledi-Geraru, Afar, Ethiopia. *Science* **347**, 1352–1355 (2015).
59. Harmann, S. et al. 3.3-million-year-old stone tools from Lomekwi 3, West Turkana, Kenya. *Nature* **521**, 310–315 (2015).
60. Leakey, M. G. et al. New hominin genus from eastern Africa shows diverse middle Pliocene lineages. *Nature* **410**, 433–440 (2001).
61. Brown, B., Brown, F. H. & Walker, A. New hominids from the Lake Turkana Basin, Kenya. *J. Hum. Evol.* **41**, 29–44 (2001).

62. Braun, D. R. et al. Earliest known Oldowan artifacts at >2.58 Ma from Ledi-Geraru, Ethiopia, highlight early technological diversity. *Proc. Natl Acad. Sci. USA* **116**, 11712–11717 (2019).
63. Lepre, C. J. et al. An earlier origin for the Acheulian. *Nature* **477**, 82–85 (2011).
64. Gamble, C. S. *Settling the Earth: the Archaeology of Deep Human History* (Cambridge Univ. Press, 2013).
65. Hlubik, S., Berna, F., Feibel, C., Braun, D. & Harris, J. W. K. Researching the nature of fire at 1.5 Mya on the site of FxJj20 AB, Koobi Fora, Kenya, using high-resolution spatial analysis and FTIR spectrometry. *Curr. Anthropol.* **58**, S243–S257 (2017).
66. Hlubik, S. et al. Hominin fire use in the Okote member at Koobi Fora, Kenya: new evidence for the old debate. *J. Hum. Evol.* **133**, 214–229 (2019).
67. Gowlett, J. A. J. The discovery of fire by humans: a long and convoluted process. *Philos. Trans. R. Soc. B* **371**, 20150164 (2016).
68. Wrangham, R. W., Jones, J. H., Laden, G., Pilbeam, D. & Conklin-Brittain, N. The raw and the stolen: cooking and the ecology of human origins. *Curr. Anthropol.* **40**, 567–594 (1999).
69. Fonseca-Azevedo, K. & Herculano-Houzel, S. Metabolic constraint imposes tradeoff between body size and number of brain neurons in human evolution. *Proc. Natl Acad. Sci. USA* **109**, 18571–18576 (2012).
70. Carmody, R. N., Weintraub, G. S. & Wrangham, R. W. Energetic consequences of thermal and nonthermal food processing. *Proc. Natl Acad. Sci. USA* **108**, 19199–19203 (2011).
71. Joordens, J. C. A. et al. *Homo erectus* at Trinil on Java used shells for tool production and engraving. *Nature* **518**, 228–231 (2015).
72. Grün, R. et al. Dating the skull from Broken Hill, Zambia, and its position in human evolution. *Nature* **580**, 372–375 (2020).
73. Timmermann, A. Quantifying the potential causes of Neanderthal extinction: abrupt climate change versus competition and interbreeding. *Quat. Sci. Rev.* **238**, 106331 (2020).
74. Banks, W. E. et al. Neanderthal extinction by competitive exclusion. *PLoS ONE* **3**, e3972 (2008).
75. Kochiyama, T. et al. Reconstructing the Neanderthal brain using computational anatomy. *Sci. Rep.* **8**, 6296 (2018).
76. Hershkovitz, I. et al. The earliest modern humans outside Africa. *Science* **359**, 456–459 (2018).
77. Harvati, K. et al. Apidima Cave fossils provide earliest evidence of *Homo sapiens* in Eurasia. *Nature* **571**, 500–504 (2019).
78. Hovers, E. in *When Neandertals and Moderns Meet* (ed. Conard, N.) 65–85 (Kerns Verlag, 2006).
79. Scerri, E. M. L., Chikhi, L. & Thomas, M. G. Beyond multiregional and simple out-of-Africa models of human evolution. *Nat. Ecol. Evol.* **3**, 1370–1372 (2019).
80. Proctor, C., Douka, K., Proctor, J. W. & Higham, T. The age and context of the KC4 Maxilla, Kent's Cavern, UK. *Eur. J. Archaeol.* **20**, 74–97 (2017).
81. Villa, P. & Roebroeks, W. Neandertal demise: an archaeological analysis of the modern human superiority complex. *PLoS ONE* **9**, 96424 (2014).
82. Galway-Witham, J., Cole, J. & Stringer, C. Aspects of human physical and behavioural evolution during the last 1 million years. *J. Quat. Sci.* **34**, 355–378 (2019).
83. Downey, G. & Lende, D. H. in *The Encultured Brain: an Introduction to Neuroanthropology* (eds Lenne, D. H. & Downey, G.) 103–138 (MIT Press, 2012).
84. Boivin, N. L. et al. Ecological consequences of human niche construction: examining long-term anthropogenic shaping of global species distributions. *Proc. Natl Acad. Sci. USA* **113**, 6388–6396 (2016).
85. Kendal, J., Tehrani, J. J. & Odling-Smeek, J. Human niche construction in interdisciplinary focus. *Philos. Trans. R. Soc. B* **366**, 785–792 (2011).
86. Potts, R. Evolution and environmental change in early human prehistory. *Annu. Rev. Anthropol.* **41**, 151–167 (2012).
87. Scerri, E. M. L. et al. Did our species evolve in subdivided populations across Africa, and why does it matter? *Trends Ecol. Evol.* **33**, 582–594 (2018).
88. Sol, D., Bacher, S., Reader, S. M. & Lefebvre, L. Brain size predicts the success of mammal species introduced into novel environments. *Am. Nat.* **172**, 63–71 (2008).
89. Potts, R. Hominin evolution in settings of strong environmental variability. *Quat. Sci. Rev.* **73**, 1–13 (2013).
90. Wedage, O. et al. Specialized rainforest hunting by *Homo sapiens* ~45,000 years ago. *Nat. Commun.* **10**, 739 (2019).
91. Roberts, P. & Stewart, B. A. Defining the ‘generalist specialist’ niche for Pleistocene *Homo sapiens*. *Nat. Hum. Behav.* **2**, 542–550 (2018).
92. Van Heteren, A. H. & Sankhyan, A. R. in *Asian Perspectives on Human Evolution* (ed. Sankhyan, A. R.) 172–187 (Serials Publications, 2009).
93. Diniz-Filho, J. A. F. & Raia, P. Island rule, quantitative genetics and brain-body size evolution in *Homo floresiensis*. *Proc. R. Soc. B* **284**, 20171065 (2017).
94. Kubo, D., Kono, R. T. & Kaifu, Y. Brain size of *Homo floresiensis* and its evolutionary implications. *Proc. R. Soc. B* **280**, 20130338 (2013).
95. Dennell, R. W., Louys, J., O'Regan, H. J. & Wilkinson, D. M. The origins and persistence of *Homo floresiensis* on Flores: biogeographical and ecological perspectives. *Quat. Sci. Rev.* **96**, 98–107 (2014).
96. Foster, J. B. Evolution of mammals on Islands. *Nature* **202**, 234–235 (1964).
97. Brown, P. et al. A new small-bodied hominin from the Late Pleistocene of Flores, Indonesia. *Nature* **431**, 1055–1061 (2004).
98. Argue, D., Groves, C. P., Lee, M. S. Y. & Junger, W. L. The affinities of *Homo floresiensis* based on phylogenetic analyses of cranial, dental, and postcranial characters. *J. Hum. Evol.* **107**, 107–133 (2017).
99. Brumm, A. et al. Early stone technology on Flores and its implications for *Homo floresiensis*. *Nature* **441**, 624–628 (2006).
100. Moore, M. W. & Brumm, A. in *Interdisciplinary Approaches to the Oldowan* (eds Hovers, E. & Braun, D. R.) 61–69 (Springer, 2009); [https://doi.org/10.1007/978-1-4020-9060-8\\_6](https://doi.org/10.1007/978-1-4020-9060-8_6)
101. Garvin, H. M. et al. Body size, brain size, and sexual dimorphism in *Homo naledi* from the Dinaledi Chamber. *J. Hum. Evol.* **111**, 119–138 (2017).
102. Laird, M. F. et al. The skull of *Homo naledi*. *J. Hum. Evol.* **104**, 100–123 (2017).
103. Holloway, R. L. et al. Endocast morphology of *Homo naledi* from the Dinaledi Chamber, South Africa. *Proc. Natl Acad. Sci. USA* **115**, 5738–5743 (2018).
104. Kivell, T. L. et al. The hand of *Homo naledi*. *Nat. Commun.* **6**, 8431 (2015).
105. Marchi, D. et al. The thigh and leg of *Homo naledi*. *J. Hum. Evol.* **104**, 174–204 (2017).
106. Dirks, P. H. et al. The age of *Homo naledi* and associated sediments in the Rising Star Cave, South Africa. *eLife* **6**, e24231 (2017).
107. Aiello, L. C. & Wheeler, P. The expensive-tissue hypothesis: the brain and the digestive system in human and primate evolution. *Curr. Anthropol.* **36**, 199–221 (1995).
108. Isler, K. & van Schaik, C. P. The expensive brain: a framework for explaining evolutionary changes in brain size. *J. Hum. Evol.* **57**, 392–400 (2009).
109. Isler, K. & Van Schaik, C. P. Metabolic costs of brain size evolution. *Biol. Lett.* **2**, 557–560 (2006).
110. Berthaume, M. A., Delezenne, L. K. & Kupczik, K. Dental topography and the diet of *Homo naledi*. *J. Hum. Evol.* **118**, 14–26 (2018).
111. Nascimento, F. F., Reis, M., Dos & Yang, Z. A biologist's guide to Bayesian phylogenetic analysis. *Nat. Ecol. Evol.* **1**, 1446–1454 (2017).
112. O'Reilly, J. E., dos Reis, M. & Donoghue, P. C. J. Dating tips for divergence-time estimation. *Trends Genet.* **31**, 637–650 (2015).
113. Yang, Z. & Donoghue, P. C. J. Dating species divergences using rocks and clocks. *Philos. Trans. R. Soc. B* **371**, 20150126 (2016).
114. Cameron, D. W. & Groves, C. P. *Bones, Stones and Molecules: Out of Africa and Human Origins* (Elsevier, 2004).
115. Cameron, D., Patnaik, R. & Sahni, A. The phylogenetic significance of the middle pleistocene Narmada hominin cranium from central India. *Int. J. Osteoarchaeol.* **14**, 419–447 (2004).
116. Berger, L. R. et al. *Australopithecus sediba*: a new species of *Homo*-like australopith from South Africa. *Science* **328**, 195–204 (2010).
117. Irish, J. D., Guatelli-Steinberg, D., Legge, S. S., De Ruiter, D. J. & Berger, L. R. Dental morphology and the phylogenetic ‘place’ of *Australopithecus sediba*. *Science* **340**, 1233062 (2013).
118. Lordkipanidze, D. et al. A complete skull from Dmanisi, Georgia, and the evolutionary biology of early *Homo*. *Science* **342**, 326–331 (2013).
119. Kimbel, W. H., Rak, Y. & Johanson, D. C. *The Skull of Australopithecus afarensis* (Oxford Univ. Press, 2004); <https://doi.org/10.5860/choice.42-1028>
120. Strait, D. S. & Grine, F. E. Inferring hominoid and early hominid phylogeny using craniodontal characters: the role of fossil taxa. *J. Hum. Evol.* **47**, 399–452 (2004).
121. Chang, M. L. *Neandertal origins, Middle Pleistocene Systematics, and Tests of Current Taxonomic and Phylogenetic Hypotheses*. PhD thesis, Univ. of Pennsylvania (2005).
122. Martíñon-Torres, M. et al. Dental evidence on the hominin dispersals during the Pleistocene. *Proc. Natl Acad. Sci. USA* **104**, 13279–13282 (2007).
123. Gilbert, W. H. in *Homo erectus: Pleistocene Evidence from the Middle Awash, Ethiopia* (eds Gilbert, W. H. & Asfaw, B.) 265–311 (Univ. of California Press, 2008).
124. Argue, D., Morwood, M. J., Sutikna, T., Jatmiko, & Saptoyo, E. W. *Homo floresiensis*: a cladistic analysis. *J. Hum. Evol.* **57**, 623–639 (2009).
125. Mounier, A., Marchal, F. & Condemi, S. Is *Homo heidelbergensis* a distinct species? New insight on the Mauer mandible. *J. Hum. Evol.* **56**, 219–246 (2009).
126. Zeitoun, V. *The Human Canopy: Homo erectus, Homo soloensis, Homo pekinensis and Homo floresiensis* (B.A.R. S1937, 2009).
127. Monge, C. S., Strait, D. S. & Grine, F. E. Expanded character sampling underscores phylogenetic stability of *Ardipithecus ramidus* as a basal hominin. *J. Hum. Evol.* **131**, 28–39 (2019).

128. Martin, J. M. et al. Drimolen cranium DNH 155 documents microevolution in an early hominin species. *Nat. Ecol. Evol.* **5**, 38–45 (2021).
129. Finstermeier, K. et al. A mitogenomic phylogeny of living primates. *PLoS ONE* **8**, 69504 (2013).
130. Kumar, S., Stecher, G., Li, M., Knyaz, C. & Tamura, K. MEGA X: molecular evolutionary genetics analysis across computing platforms. *Mol. Biol. Evol.* **35**, 1547–1549 (2018).
131. Lanfear, R., Frandsen, P. B., Wright, A. M., Senfeld, T. & Calcott, B. Partitionfinder 2: new methods for selecting partitioned models of evolution for molecular and morphological phylogenetic analyses. *Mol. Biol. Evol.* **34**, 772–773 (2017).
132. Lanfear, R., Calcott, B., Ho, S. Y. W. & Guindon, S. PartitionFinder: combined selection of partitioning schemes and substitution models for phylogenetic analyses. *Mol. Biol. Evol.* **29**, 1695–1701 (2012).
133. Lewis, P. A likelihood approach to estimating phylogeny from discrete morphological character data. *Soc. Syst. Biol.* **50**, 913–925 (2001).
134. Püschel, H. P., O'Reilly, J. E., Pisani, D. & Donoghue, P. C. J. The impact of fossil stratigraphic ranges on tip-calibration, and the accuracy and precision of divergence time estimates. *Palaeontology* **63**, 67–83 (2020).
135. Katoh, S. et al. New geological and palaeontological age constraint for the gorilla-human lineage split. *Nature* **530**, 215–218 (2016).
136. Kunimatsu, Y. et al. A new Late Miocene great ape from Kenya and its implications for the origins of African great apes and humans. *Proc. Natl Acad. Sci. USA* **104**, 19220–19225 (2007).
137. Begun, D. R. Miocene hominids and the origins of the African apes and humans. *Annu. Rev. Anthropol.* **39**, 67–84 (2010).
138. Begun, D. R., Nargolwalla, M. C. & Kordos, L. European Miocene hominids and the origin of the African ape and human clade. *Evol. Anthropol.* **21**, 10–23 (2012).
139. Suwa, G., Kono, R. T., Katoh, S., Asfaw, B. & Beyene, Y. A new species of great ape from the late Miocene epoch in Ethiopia. *Nature* **448**, 921–924 (2007).
140. Harrison, T. in *Cenozoic Mammals of Africa* (eds Werdelin, L. & Sanders, W.) 429–470 (Univ. of California Press, 2012); <https://doi.org/10.1525/california/9780520257214.003.0024>
141. Fu, Q. et al. Genome sequence of a 45,000-year-old modern human from western Siberia. *Nature* **514**, 445–449 (2014).
142. Fu, Q. et al. A revised timescale for human evolution based on ancient mitochondrial genomes. *Curr. Biol.* **23**, 553–559 (2013).
143. Berger, L. R., Hawks, J., Dirks, P. H. G. M., Elliott, M. & Roberts, E. M. *Homo naledi* and Pleistocene hominin evolution in subequatorial Africa. *eLife* **6**, e24234 (2017).
144. Kimbel, W. H. & Rak, Y. *Australopithecus sediba* and the emergence of *Homo*: questionable evidence from the cranium of the juvenile holotype MH 1. *J. Hum. Evol.* **107**, 94–106 (2017).
145. Schroeder, L. et al. Skull diversity in the *Homo* lineage and the relative position of *Homo naledi*. *J. Hum. Evol.* **104**, 124–135 (2017).
146. Ronquist, F. et al. MrBayes 3.2: efficient Bayesian phylogenetic inference and model choice across a large model space. *Syst. Biol.* **61**, 539–542 (2012).
147. Miller, M. A., Pfeiffer, W. & Schwartz, T. Creating the CIPRES Science Gateway for inference of large phylogenetic trees. In *Proc. Gateway Computing Environments Workshop (GCE)* 1–8 (IEEE, 2010); <https://doi.org/10.1109/GCE.2010.5676129>
148. Rambaut, A., Drummond, A. J., Xie, D., Baele, G. & Suchard, M. A. Posterior summarization in Bayesian phylogenetics using Tracer 1.7. *Syst. Biol.* **67**, 901–904 (2018).
149. Zhang, C., Stadler, T., Klopstein, S., Heath, T. A. & Ronquist, F. Total-evidence dating under the fossilized birth–death process. *Syst. Biol.* **65**, 228–249 (2016).
150. Jerison, H. J. *Evolution of the Brain and Intelligence* (Academic Press, 1973).
151. Jerison, H. J. Brain, body and encephalization in early primates. *J. Hum. Evol.* **8**, 615–635 (1979).
152. Cairó, O. External measures of cognition. *Front. Hum. Neurosci.* **5**, 108 (2011).
153. Stephan, H., Frahm, H. D. & Baron, G. New and revised data on volumes of brain structures in insectivores and primates. *Folia Primatol.* **35**, 1–29 (1981).
154. R. Core Team *R: A Language and Environment for Statistical Computing* (R Foundation for Statistical Computing, 2019).
155. Paradis, E., Claude, J. & Strimmer, K. APE: analyses of phylogenetics and evolution in R language. *Bioinformatics* **20**, 289–290 (2004).
156. Pinheiro, J., Bates, D., DebRoy, S. & Sarkar, D. nlme: linear and nonlinear mixed effects models. R package version 3.1-147 (2020).
157. Ives, A. R. R 2 s for correlated data: phylogenetic models, LMMs, and GLMMs. *Syst. Biol.* **68**, 234–251 (2019).
158. Revell, L. J. phytols: an R package for phylogenetic comparative biology (and other things). *Methods Ecol. Evol.* **3**, 217–223 (2012).

## Acknowledgements

This research was funded by the National Agency for Research and Development (ANID)/PIFCHA/Doctorado en el extranjero Becas Chile/2018-72190003 to H.P.P.; a Marie Skłodowska-Curie Actions Individual Fellowship (H2020-MSCA-IF-2018-2020; no. 792611) and the European Research Council (ERC) starting grant PalM, under the European Union's Horizon 2020 Research and Innovation Programme (no. 756226) to O.C.B.; and the Leverhulme Trust Early Career Fellowship, ECF-2018-264 to T.A.P.

## Author contributions

H.P.P. and T.A.P. conceived and designed the study. O.C.B. compiled the body mass and ECV dataset. J.E.O. provided methodological support. H.P.P. and T.A.P. carried out all the mentioned analyses and wrote an initial draft. H.P.P., O.C.B., J.E.O., R.B. and T.A.P. interpreted the obtained results and contributed to the writing of the submitted version of this work.

## Competing interests

The authors declare no competing interests.

## Additional information

**Extended data** is available for this paper at <https://doi.org/10.1038/s41559-021-01431-1>.

**Supplementary information** The online version contains supplementary material available at <https://doi.org/10.1038/s41559-021-01431-1>.

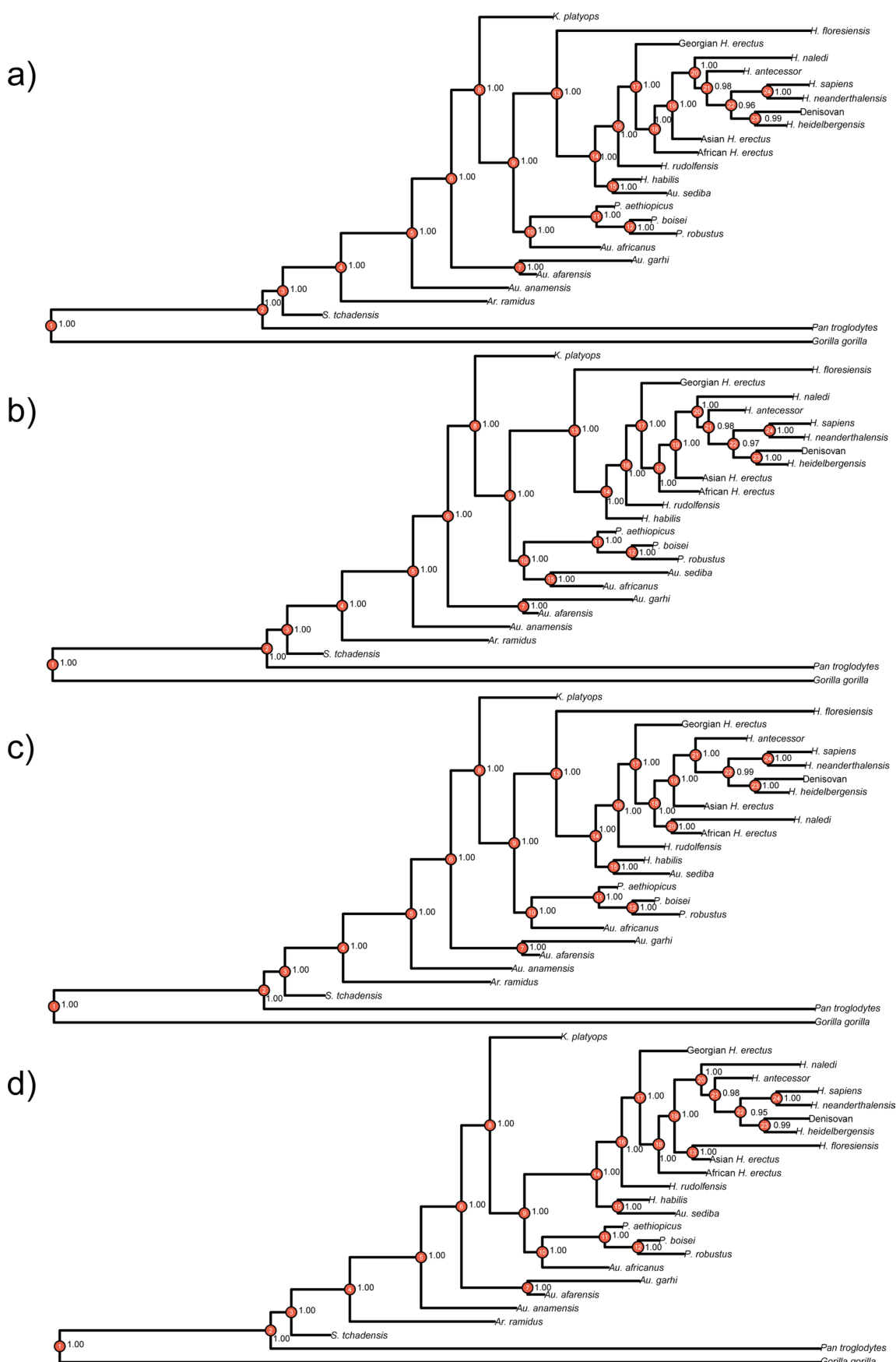
**Correspondence and requests for materials** should be addressed to H.P.P. or T.A.P.

**Peer review information** *Nature Ecology & Evolution* thanks Fredrik Ronquist and the other, anonymous, reviewer(s) for their contribution to the peer review of this work. Peer reviewer reports are available.

**Reprints and permissions information** is available at [www.nature.com/reprints](http://www.nature.com/reprints).

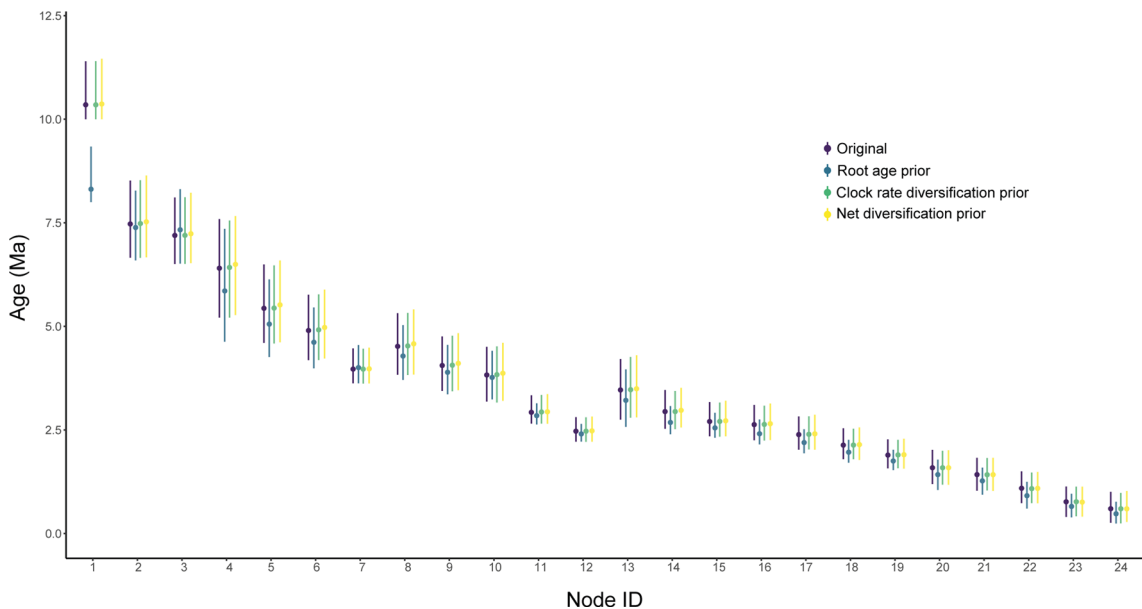
**Publisher's note** Springer Nature remains neutral with regard to jurisdictional claims in published maps and institutional affiliations.

© The Author(s), under exclusive licence to Springer Nature Limited 2021

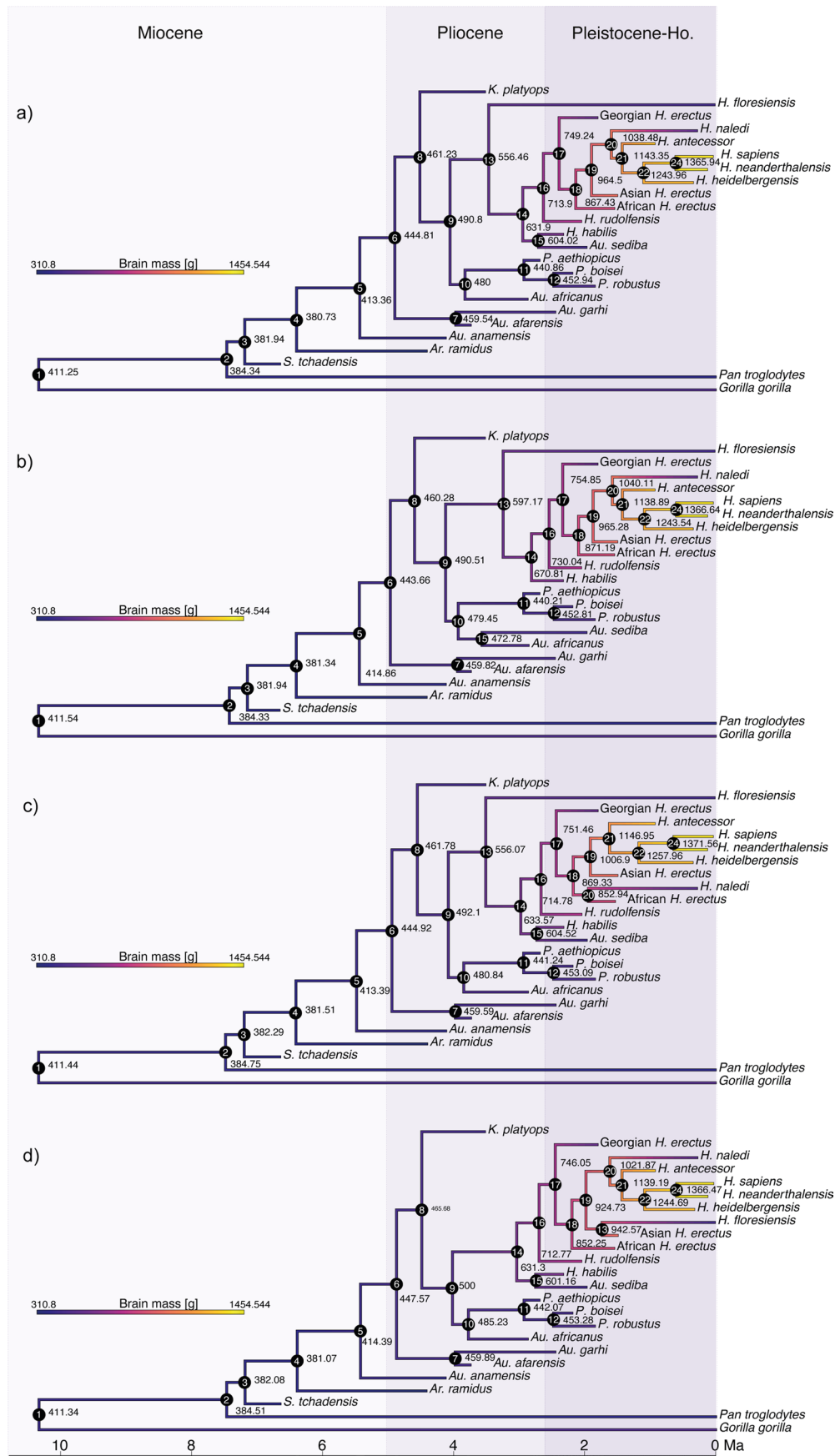


**Extended Data Fig. 1 | See next page for caption.**

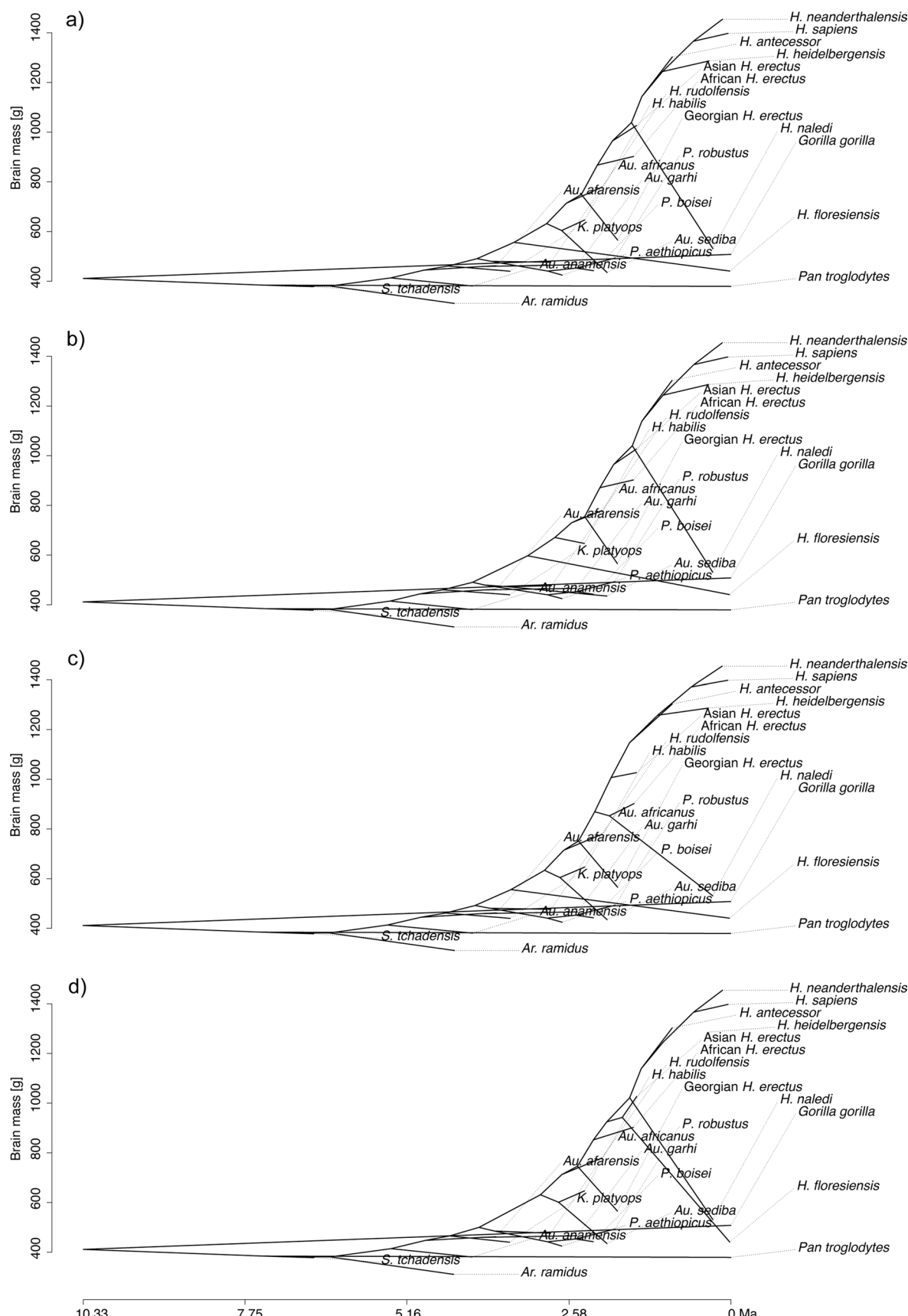
**Extended Data Fig. 1 | Consensus trees with Bayesian posterior probabilities showing the support for the nodes.** **a**, Dembo *et al.*<sup>17</sup> hypothesis, **b**, *Au. sediba* hypothesis, **c**, *H. naledi* hypothesis and **d**, *H. floresiensis* hypothesis. Node numbers mentioned in text are within the red circles. We used soft constraints to allow the unconstrained taxa (that is, *H. sapiens*, *H. neanderthalensis*, *H. heidelbergensis* and Denisovans) to change position freely within the tree. For more details about the constraints used, see the Methods section.



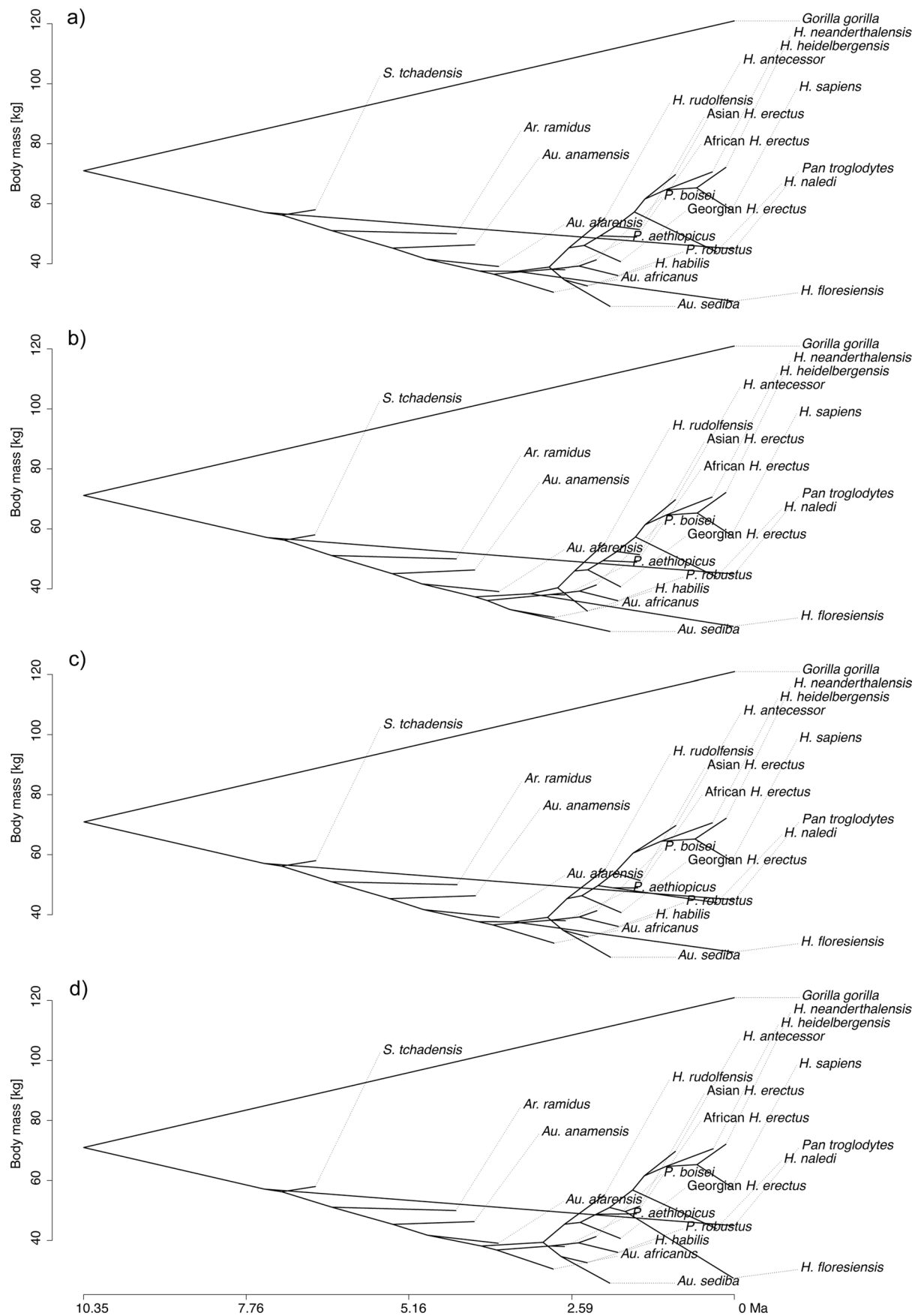
**Extended Data Fig. 2 | Prior sensitivity analysis.** The dots indicate the mean and the lines the associated 95% highest posterior density interval (HPD) of the divergence-time estimations for each node. Different colours indicate the different priors that were tested. See the Methods for further details about each one of the priors that were tested.



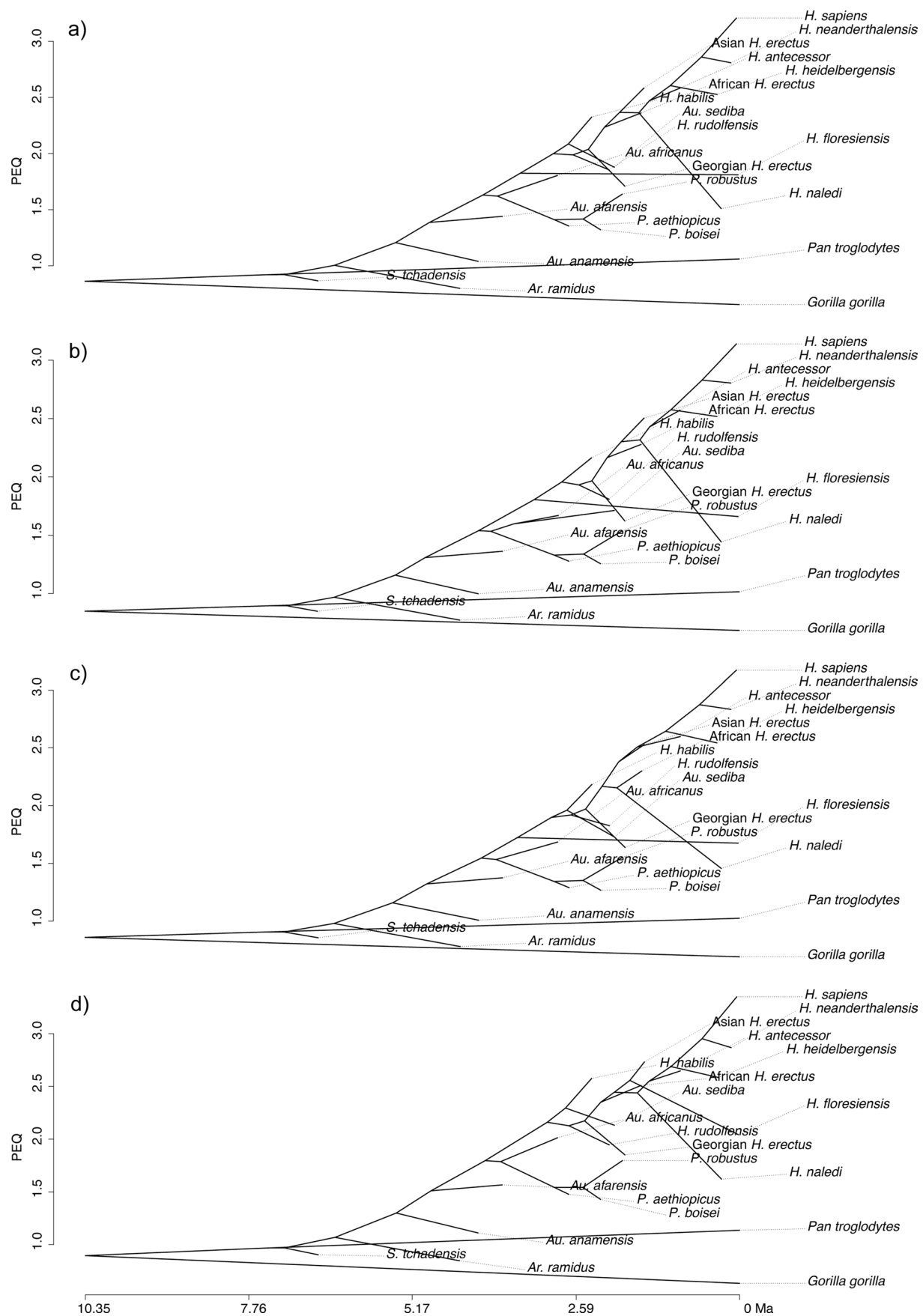
**Extended Data Fig. 3 | Brain mass ACSR for each species mapped onto the four consensus time-calibrated phylogenies.** **a**, Dembo *et al.*<sup>17</sup> hypothesis, **b**, *Au. sediba* hypothesis, **c**, *H. naledi* hypothesis and **d**, *H. floresiensis* hypothesis. The ACSR values were reconstructed using a ML ancestral character estimation method under a Brownian motion model.



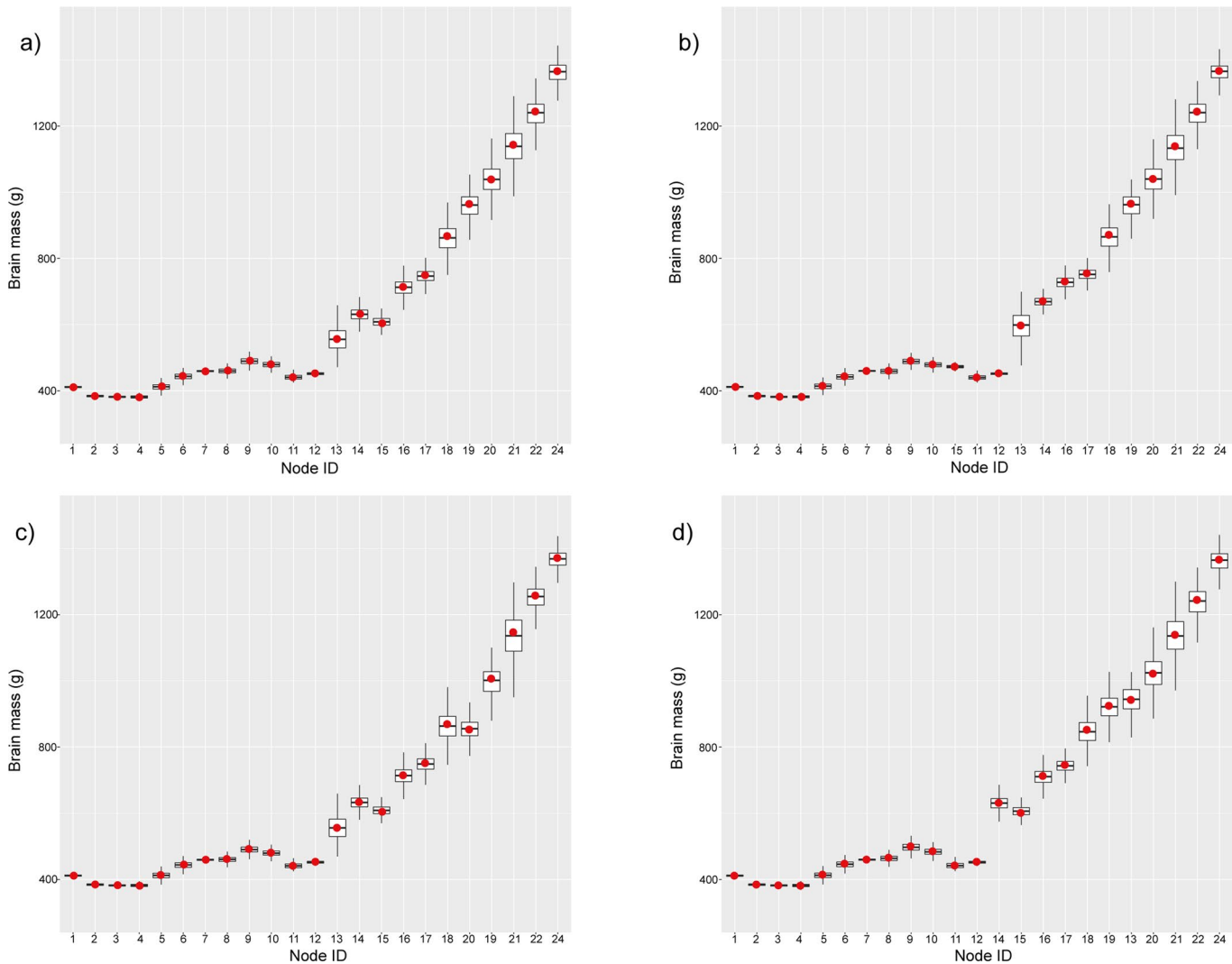
**Extended Data Fig. 4 | Brain mass (g) ACSR traitgram for each species mapped onto the four consensus time-calibrated phylogenies.** **a**, Dembo et al.<sup>17</sup> hypothesis, **b**, *Au. sediba* hypothesis, **c**, *H. naledi* hypothesis and **d**, *H. floresiensis* hypothesis.



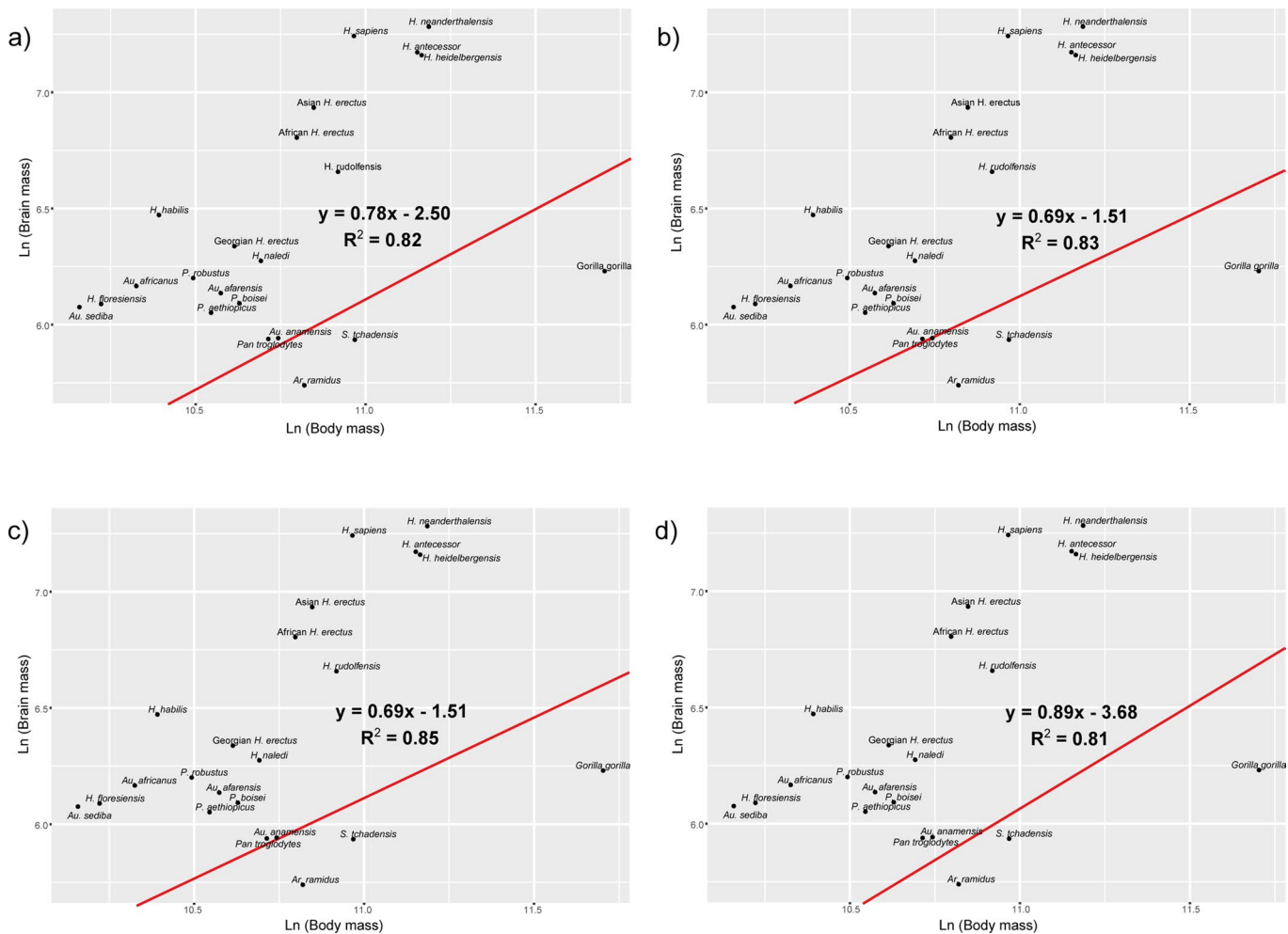
**Extended Data Fig. 5 | Body mass (kg) ACSR traitgram for each species mapped onto the four consensus time-calibrated phylogenies. a, Dembo et al.<sup>17</sup> hypothesis, b, *Au. sediba* hypothesis, c, *H. naledi* hypothesis and d, *H. floresiensis* hypothesis.**



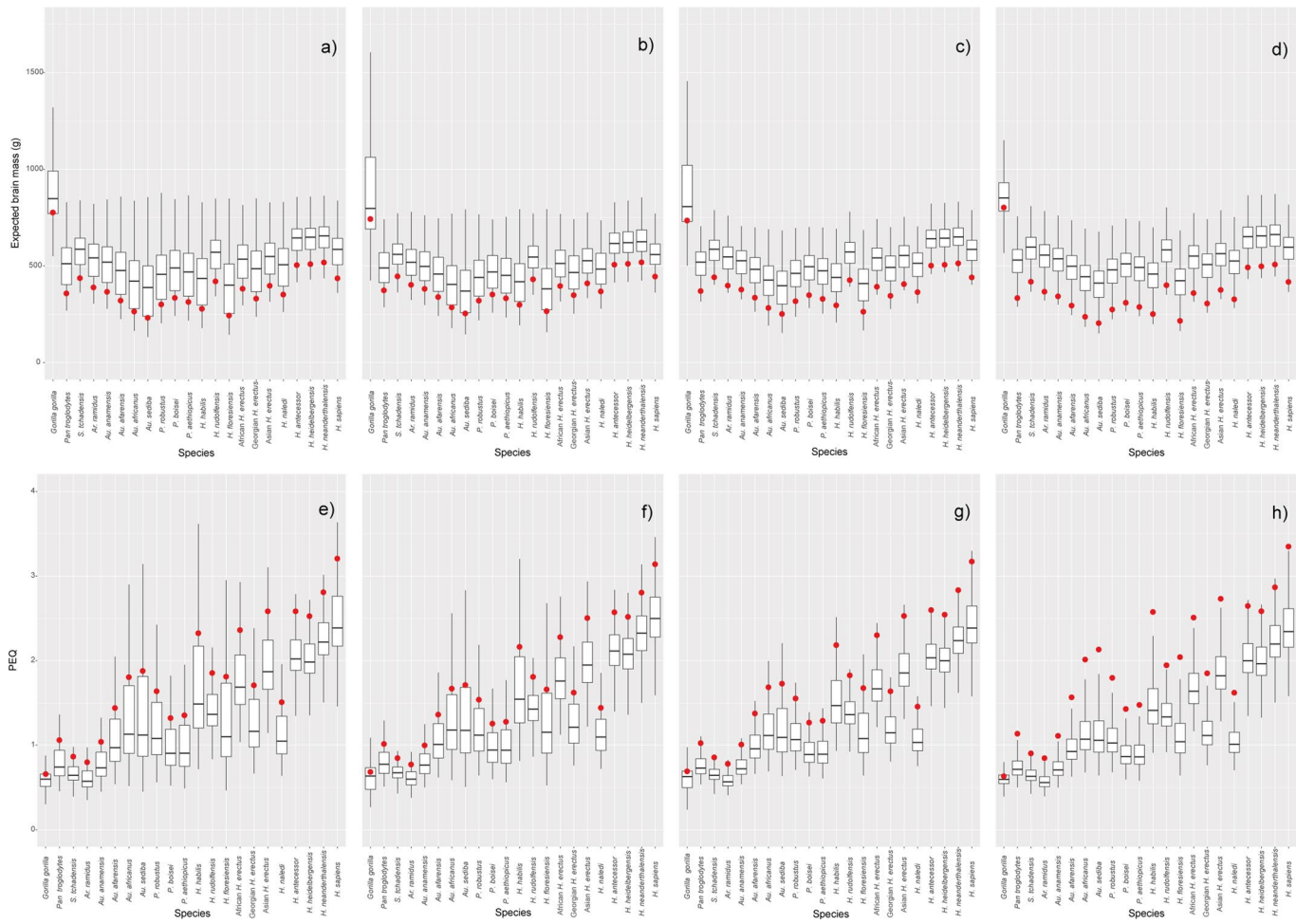
**Extended Data Fig. 6 | PEQ ACSR traitgram for each species mapped onto the four consensus time-calibrated phylogenies.** **a**, Dembo et al.<sup>17</sup> hypothesis, **b**, *Au. sediba* hypothesis, **c**, *H. naledi* hypothesis and **d**, *H. floresiensis* hypothesis.



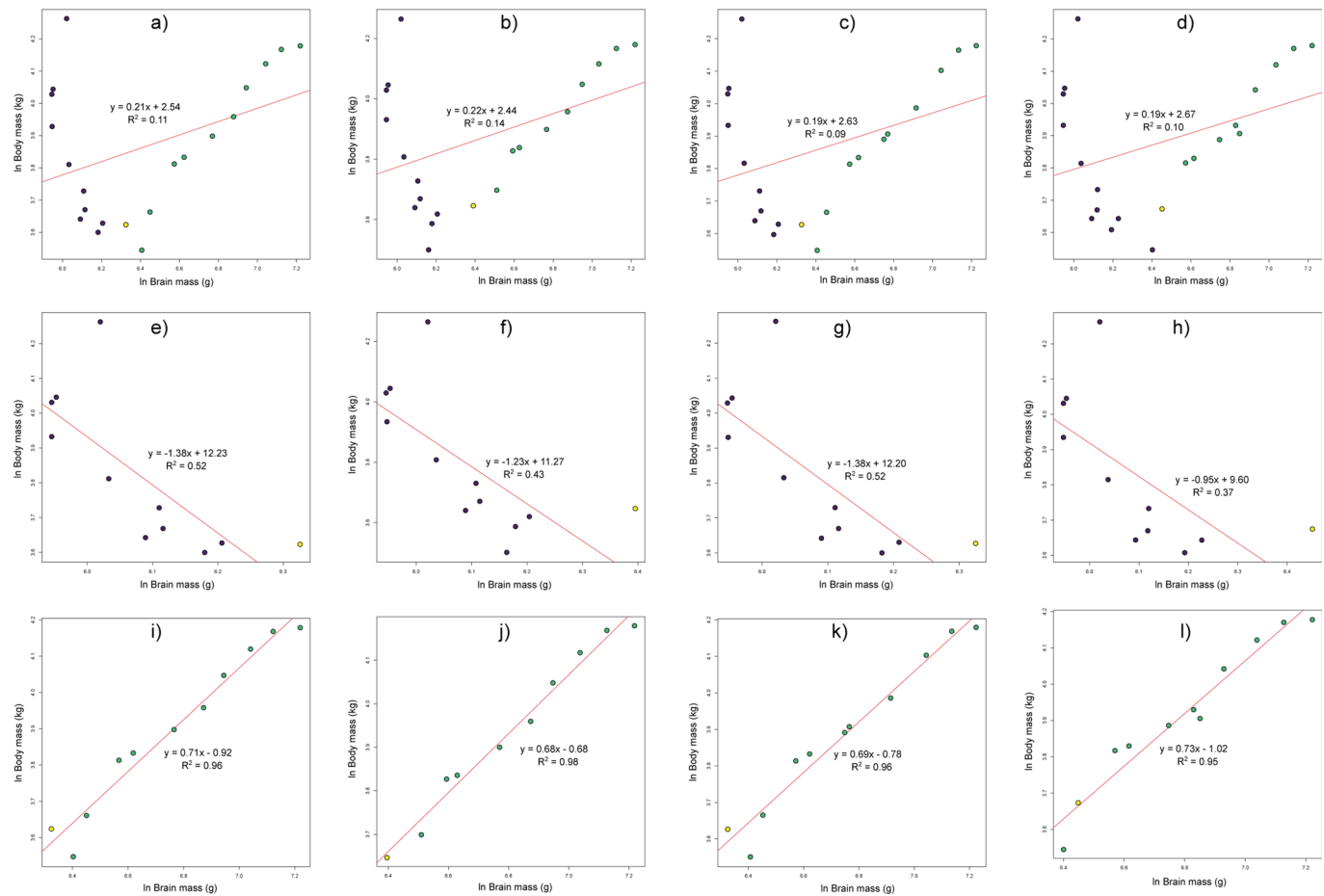
**Extended Data Fig. 7 | Boxplots of brain mass (g) ACSR per node based on a sample of 9002 time-calibrated posterior trees for each one of the plots.**  
**a**, Dembo *et al.*<sup>17</sup> hypothesis, **b**, *Au. sediba* hypothesis, **c**, *H. naledi* hypothesis and **d**, *H. florensis* hypothesis. The red dots indicate the brain mass (g) ACSR conducted using the consensus trees (as in Extended Data Fig. 3). The median is indicated by the horizontal black line, the interquartile range (IQR) is the white box and the whiskers indicate the minimum and the maximum (at  $1.5 \times \text{IQR}$  of the lower and upper hinge respectively). For details of each node, see Fig. 2.



**Extended Data Fig. 8 | PGLS models of ln(body mass) on ln(brain mass) based on the different consensus trees. a,** Dembo et al.<sup>17</sup> hypothesis, **b,** *Au. sediba* hypothesis, **c,** *H. naledi* hypothesis and **d,** *H. floresiensis* hypothesis. We used a generalised least-squares fit by restricted maximum likelihood (REML), and a Brownian motion correlation structure. The resulting equations and  $R^2$  are in the plots next to the regression line in red.



**Extended Data Fig. 9 | Boxplots of expected brain mass (a-d) and PEQ (e-h) for all the tips based on a sample of 9002 time-calibrated posterior trees for each one of the hypotheses.** **a,e**, Dembo *et al.*<sup>17</sup> hypothesis; **b,f**, *Au. sediba* hypothesis; **c,g**, *H. naledi* hypothesis and **d,h**, *H. floresiensis* hypothesis. The red dots indicate the expected brain mass (in g) for the tips of the consensus trees (**a-d**), or alternatively, the PEQ calculated for the tips of the consensus trees (**e-h**). The median is indicated by the horizontal black line, the interquartile range (IQR) is the white box and the whiskers indicate the minimum and the maximum (at 1.5 \* IQR of the lower and upper hinge respectively). Further details about the hypotheses and how the expected brain mass and the PEQ were calculated are provided in the Methods section.



**Extended Data Fig. 10 | Brain mass ACSR versus body mass ACSR regressions from the consensus trees for each one of hypotheses. a-d, Regressions considering nodes 1 to 24, e-h, regressions considering nodes 1 to 13 and i-l, regressions considering nodes 13 to 24. a,e,i, Dembo et al.<sup>17</sup> hypothesis; b,f,j, Au. sediba hypothesis; c,g,k, H. naledi hypothesis and d,h,l, H. floresiensis hypothesis. The regression equations and the R<sup>2</sup> values are given next to the regression's lines in red. Colours dark purple, yellow and green indicate nodes 1 to 12, node 13 and nodes 14 to 24, respectively. In the case of the H. floresiensis hypothesis, node 14 was highlighted in yellow instead of node 13 due changes in the position of this node for this hypothesis. Nodes 7, 8 and 23 are not considered due the lack of body mass and/or brain mass estimations.**

## Reporting Summary

Nature Research wishes to improve the reproducibility of the work that we publish. This form provides structure for consistency and transparency in reporting. For further information on Nature Research policies, see our [Editorial Policies](#) and the [Editorial Policy Checklist](#).

### Statistics

For all statistical analyses, confirm that the following items are present in the figure legend, table legend, main text, or Methods section.

n/a Confirmed

- The exact sample size ( $n$ ) for each experimental group/condition, given as a discrete number and unit of measurement
- A statement on whether measurements were taken from distinct samples or whether the same sample was measured repeatedly
- The statistical test(s) used AND whether they are one- or two-sided  
*Only common tests should be described solely by name; describe more complex techniques in the Methods section.*
- A description of all covariates tested
- A description of any assumptions or corrections, such as tests of normality and adjustment for multiple comparisons
- A full description of the statistical parameters including central tendency (e.g. means) or other basic estimates (e.g. regression coefficient) AND variation (e.g. standard deviation) or associated estimates of uncertainty (e.g. confidence intervals)
- For null hypothesis testing, the test statistic (e.g.  $F$ ,  $t$ ,  $r$ ) with confidence intervals, effect sizes, degrees of freedom and  $P$  value noted  
*Give  $P$  values as exact values whenever suitable.*
- For Bayesian analysis, information on the choice of priors and Markov chain Monte Carlo settings
- For hierarchical and complex designs, identification of the appropriate level for tests and full reporting of outcomes
- Estimates of effect sizes (e.g. Cohen's  $d$ , Pearson's  $r$ ), indicating how they were calculated

*Our web collection on [statistics for biologists](#) contains articles on many of the points above.*

### Software and code

Policy information about [availability of computer code](#)

Data collection	All the data analysed in this work was available online. Morphological data was obtained from the literature, whilst mtDNA data was downloaded from GenBank. In addition, all the data and code used in this paper are available in a permanent Zenodo repository at <a href="https://dx.doi.org/10.5281/zenodo.4537445">https://dx.doi.org/10.5281/zenodo.4537445</a> and on GitHub at <a href="https://github.com/HansPueschel/Hominin-div-time-evolution">https://github.com/HansPueschel/Hominin-div-time-evolution</a> .
Data analysis	We aligned the sequences by MUSCLE using MEGA X v10.0.4. We performed the Bayesian analysis with MrBayes v3.2.7a on CIPRES portal v 3.3. The programme Tracer v1.7.150 was used to check the obtained results. When analysing PEQ and body mass, we used R v3.6.1 and the packages 'ape' v5.3 and 'nlme' v3.1-142. We used a maximum likelihood approach to reconstruct the ancestral character states at the internal nodes of the phylogenetic tree using the package 'phytools' v0.6-99. In addition, all the data and code used in this paper are available in a permanent Zenodo repository at <a href="https://dx.doi.org/10.5281/zenodo.4537445">https://dx.doi.org/10.5281/zenodo.4537445</a> and on GitHub at <a href="https://github.com/HansPueschel/Hominin-div-time-evolution">https://github.com/HansPueschel/Hominin-div-time-evolution</a> .

For manuscripts utilizing custom algorithms or software that are central to the research but not yet described in published literature, software must be made available to editors and reviewers. We strongly encourage code deposition in a community repository (e.g. GitHub). See the Nature Research [guidelines for submitting code & software](#) for further information.

## Data

Policy information about [availability of data](#)

All manuscripts must include a [data availability statement](#). This statement should provide the following information, where applicable:

- Accession codes, unique identifiers, or web links for publicly available datasets
- A list of figures that have associated raw data
- A description of any restrictions on data availability

All data analysed in this study are available in the Supplementary information (Supplementary Tables 2 and 3) and in a permanent Zenodo (zenodo.org) repository at <https://dx.doi.org/10.5281/zenodo.4537445>. Additionally, the data is available in an open access repository: <https://github.com/HansPueschel/Hominin-div-time-evolution>.

## Field-specific reporting

Please select the one below that is the best fit for your research. If you are not sure, read the appropriate sections before making your selection.

Life sciences       Behavioural & social sciences       Ecological, evolutionary & environmental sciences

For a reference copy of the document with all sections, see [nature.com/documents/nr-reporting-summary-flat.pdf](https://nature.com/documents/nr-reporting-summary-flat.pdf)

## Ecological, evolutionary & environmental sciences study design

All studies must disclose on these points even when the disclosure is negative.

Study description

We applied a Bayesian Total Evidence Dating approach to a recent hominin phylogeny, estimating that the origin of Homo most likely occurred between 4.30 and 2.56 Ma. Then using the resultant time-scaled phylogenies we performed ancestral state reconstructions in body mass and encephalisation. Our results showed the onset of a trend towards greater body mass with the origin of the genus, and gradual but accelerating encephalisation rates throughout hominin evolution.

Research sample

The morphological data were obtained from the literature (see references in the manuscript), and corresponds to supermatrix from craniodental matrices used in 13 previous studies. The molecular data were complete mtDNA genomes extracted from GenBank of the species in which it was available: Gorilla gorilla (KF914214.1), Pan troglodytes (JF727180.2), Homo heidelbergensis (KF683087.1), Homo neanderthalensis (MK123269.1), Homo sapiens(KC417443.1) and Denisovans (KX663333.1).

Sampling strategy

For the morphological data, we selected the most complete and up-to-date hominin morphological matrix. We included mtDNA sequences from Genebank for the taxa in which it was available. In particular, we selected the sequences extracted from individuals aged equally or as close as possible to the morphologically coded fossils.

Data collection

NA

Timing and spatial scale

NA

Data exclusions

K. platyops and Au. garhi tips were dropped from the ancestral state reconstructions for body mass and PEQ as there were no body mass estimations for these taxa available due to their fragmentary fossil record. Similarly, Denisovans were removed from all ancestral state reconstructions analyses as there are no estimates available for their brain and body mass.

Reproducibility

All data analysed in this study are available in the Supplementary information (Supplementary Tables 2 and 3) and in a permanent Zenodo (zenodo.org) repository at <https://dx.doi.org/10.5281/zenodo.4537445>. Additionally, the data is available in an open access repository: <https://github.com/HansPueschel/Hominin-div-time-evolution>.

Randomization

NA

Blinding

NA

Did the study involve field work?  Yes  No

## Reporting for specific materials, systems and methods

We require information from authors about some types of materials, experimental systems and methods used in many studies. Here, indicate whether each material, system or method listed is relevant to your study. If you are not sure if a list item applies to your research, read the appropriate section before selecting a response.

**Materials & experimental systems**

n/a	Involved in the study
<input checked="" type="checkbox"/>	Antibodies
<input checked="" type="checkbox"/>	Eukaryotic cell lines
<input checked="" type="checkbox"/>	Palaeontology and archaeology
<input checked="" type="checkbox"/>	Animals and other organisms
<input checked="" type="checkbox"/>	Human research participants
<input checked="" type="checkbox"/>	Clinical data
<input checked="" type="checkbox"/>	Dual use research of concern

**Methods**

n/a	Involved in the study
<input checked="" type="checkbox"/>	ChIP-seq
<input checked="" type="checkbox"/>	Flow cytometry
<input checked="" type="checkbox"/>	MRI-based neuroimaging